Journal Pre-proofs

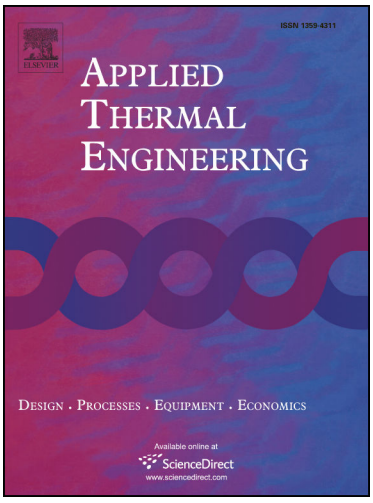

Thermodynamic Modeling of Compressed Air Energy Storage for Energy and Reserve Markets

M. Hemmati, B. Mohammadi-Ivatloo, M. Abapour, M. Shafiee

PII: S1359-4311(21)00395-1
DOI: https://doi.org/10.1016/j.applthermaleng.2021.116948
Reference: ATE 116948

To appear in: *Applied Thermal Engineering*

Received Date: 9 September 2020
Revised Date: 15 January 2021
Accepted Date: 6 April 2021

Please cite this article as: M. Hemmati, B. Mohammadi-Ivatloo, M. Abapour, M. Shafiee, Thermodynamic Modeling of Compressed Air Energy Storage for Energy and Reserve Markets, *Applied Thermal Engineering* (2021), doi: https://doi.org/10.1016/j.applthermaleng.2021.116948

Thermodynamic Modeling of Compressed Air Energy Storage for Energy and Reserve Markets

M. Hemmati[1], B. Mohammadi-Ivatloo[1,2,*], M. Abapour[1], M. Shafiee[3]

[1] Faculty of Electrical and Computer Engineering, University of Tabriz, Tabriz, Iran

[2] Department of Energy Technology, Aalborg University, Aalborg, Denmark

[3] Mechanical Engineering Division, School of Engineering, University of Kent, Canterbury, UK

Abstract

Compressed air energy storage (CAES) system is one of the highly efficient and low capital cost energy storage technologies, which is used on a large scale. However, due to multiple operational and technical limitations, the CAES operation should be incorporated with thermodynamic characteristics. Therefore, in this paper, novel thermodynamic modeling of CAES facility integrated with the hybrid thermal, wind, and photovoltaic (PV) farms to participate in energy and reserve markets is investigated. Considering the thermodynamic characteristics makes the proposed scheduling more realistic, while imposes multiple constraints on the optimal operation of the hybrid system. The operation of the CAES facility during charging and discharging modes, considering thermodynamic characteristics are analyzed simultaneously, and the state of charge of the cavern is calculated for both modes. In addition to taking into account the thermodynamic characteristics, the recovery cycle capability is embedded for the CAES facility to recover heat from the turbine in the preheater results in increased turbine efficiency. The proposed scheduling of the hybrid system is exposed by high-level uncertainty caused by energy and reserve market prices, as well as wind and PV farms power fluctuation. Hence, the scenario-based stochastic approach is applied based on real historical data of the KHAF station in IRAN to handle existing uncertainties. Numerical results are provided for different cases. The major conclusions of the numerical results show the effectiveness of the recovery cycle from profit improvement and burned fuel reduction up to 11.36% and 11.33%, respectively, while the thermodynamical constraints in the CAES performance make the realistic model, compared with the conventional CAES.

Keywords: Hybrid system, CAES facility, thermodynamic characteristic, energy and reserve markets, profit maximization, recovery cycle, scenario-based stochastic approach.

Nomenclature:

Index:

G	Index for thermal units
t	Index for times
ω	Index for scenarios
u	Index of minimum on/ off time limits from 1 to $\max\{MUT_G, MDT_G\}$

Subscripts

w	The subscript for wind power
x	The subscript for the exhaust of the turbine
b	Subscript for burner
f	Subscript for fuel

Superscript

c	Superscript for charging
d	Superscript for discharging
r	Superscript for reserve market
$curt$	Superscript for wind and solar power curtailment
exp	Superscript for expander
NG	Superscript for natural gas

Parameters:

NG	Number of thermal units
NT	Number of the time intervals
N_ω	Number of scenarios
$AM^{\max}$	A maximum air mass of cavern (kg)
$E^{\max}$	The maximum energy capacity of the cavern (MWh)
G_{ING}	Hourly irradiation (W/m^2)
G_{STC}	Standard irradiation (W/m^2)
k_1, k_2, k_3	Wind turbine generation coefficients
k'	Maximum power temperature coefficient
$P_{W_{rated}}$	Rated power generation by wind farm (MW)
P_{STC}	The power generated by the PV farm in standard condition (MW)
T_c / T_r	PV cell/ air temperature (K)
μ / σ	Mean/standard deviation of normal probability distribution function for PV power output modeling

μ_{π^e} / σ_{π^e}	Mean / standard deviation of Normal distribution function for energy and reserve prices modeling
$P^c_{\min}$ / $P^c_{\max}$	Minimum/maximum power charging by CAES (MW)
$P^{d,\exp}_{\min}$ / $P^{d,\exp}_{\max}$	Minimum/maximum discharging power by expander (MW)
$P_G^{\min}$ / $P_G^{\max}$	Minimum/maximum generated power by thermal unit *G* (MW)
T_G^{on} / T_G^{off}	Number of continuous on/off times for thermal unit *G* (hour)
V_{cut-in}/$V_{cut-out}$/V_{rated}	Cut-in/ Cut-out/ rated wind speed of turbine (m/s)
MDT_G / MUT_G	Minimum down/uptime of thermal unit *G* (hour)
C_{pv}^{curt} / C_w^{curt}	Curtailment cost of PV/ wind farm ($/MWh)
π^{NG}	Natural gas price ($/MWh)
c_p	Specific heat capacity ($kj\ /\ kg.K$)
τ_R	The time constant (*s*)
Ω_t	Pressure ratio
η_t	Efficiency (p.u.)
γ	Heat capacity ratio
ER	Energy ratio
HR^{nom}	Heat rate of CAES facility
$VOM^{\exp}$	The variable operating cost of CAES during discharging mode
VOM^c	The variable operating cost of CAES during charging mode

Variables:

ρ_ω	The probability of the scenario ω
AF^c	Airflow rate during charging (*kg/s. MW.MPa*)
AF^d	Airflow rate during discharging (kg/s. MW.MPa)
$\dot{m}_f$	Mass of fuel flow rate (kg/s)
q_0	Heat transfer (*KJ*)
$Pa_{c,t}$	Cavern pressure during charging mode at time *t* per Mega-Pascal (MPa)
$Pa_{d,t}$	Cavern pressure during discharging mode at time *t* (MPa)
Ψ / Γ	Charging/discharging function
$\Re$	The mass stored air function
T_b	The temperature of the burner (*K*)
T_x	Exhaust gas temperature (*K*)
$SoC_{t,\omega}$ / $SoC_{t-1,\omega}$	State of charge at time *t* and *t-1* and scenario ω

$P^{c}_{t,\omega}$	Power charging at time *t* and scenario ω of CAES (MW)
$P^{d}_{t,\omega} / P^{d,r}_{t,\omega}$	Power discharging to participate in energy/reserve market at time *t* and scenario ω (MW)
$SU_{G,t,\omega}, SD_{G,t,\omega}$	Start-up/shut-down cost of thermal unit *G* at time *t* and scenario ω ($/MWh)
$P_{w,t,\omega} / P_{pv,t,\omega}$	Purchased power output by wind/PV at time *t* and scenario ω in the energy market (MW)
$P^{r}_{w,t,\omega} / P^{r}_{pv,t,\omega}$	Purchased power output by wind/PV at time *t* and scenario ω in reserve market (MW)
$P^{curt}_{w,t,\omega} / P^{curt}_{pv,t,\omega}$	Wind/PV power curtailment at time *t* and scenario ω
$P_{G,t,\omega} / P^{r}_{G,t,\omega}$	Purchased generated power by thermal unit *G* to participate in energy/reserve market at time *t* and scenario ω (MW)
Z	Objective function
$F(P_{G,t,\omega})$	The cost function of thermal unit *G* at time *t* and scenario ω ($/MWh)
$\pi^{e}_{t,\omega} / \pi^{e,r}_{t,\omega}$	Energy/reserve market power price at time *t* and scenario ω ($/MWh)

Binary Variable:

$x^{c}_{t,\omega} / x^{d}_{t,\omega}$	A binary variable for charging/discharging mode at time *t* and scenario ω
$I_{G,t} / I_{G,t-1}$	The binary variable of thermal unit *G* status at time *t* /*t-1* and scenario ω

Acronym

CAES	Compressed air energy storage
NG	Natural gas
SoC	State of Charge
HR	Heat rate
MINLP	Mixed-integer linear programming

I. Introduction

The total global renewable energy share is anticipated to reach 36% by 2030 [1]. Therefore, the need for flexible emerging technology such as energy storage systems to facilitate the integration of renewable energy and key performance options for energy efficiency improvement is essential [2]. The energy storage systems are a suitable solution for mitigating the fluctuation of renewable energy in the power system [3]. Among all energy storage technologies, compressed air energy storage (CAES) is one of the large-scale and low-cost bulk energy storage systems, offering many advantages, including reliability improvement, integration of renewable energy, and energy consumption time-shifting [4, 5].

The basic CAES facility performance is the thermodynamic process, which compresses the air during charging mode and releases the high-pressure air at discharging times.

The technical and economic performance of the CAES facility is a function of its equipment characteristics (in particular, turbines and compressors), which impose the operation of the CAES facility. Several studies have developed optimal scheduling models of CAES facilities from economic and environmental points of view. The comprehensive off-design operation assessment of the tri-generation subcooled CAES facility for the various operational condition was developed by [6]. In [7] developed a clean CAES coupled with solar and wind power generators to improve the traditional CAES fossil fuel issues. The authors of [8] proposed a risk-constrained bidding/offering strategy for merchant CAES in the energy market. They considered the price forecasting error as an uncertain parameter and an information gap decision theory (IGDT) approach is used to handle it. The authors of [9] presented an adaptive self-scheduling wind power shared with the CAES facility to participate in the power market. Wind power generation and power price forecasting errors were considered as uncertain parameters, and a robust optimization approach was implemented to control these parameters. The applicability and benefits of look-ahead scheduling of the hybrid system, including wind energy, CAES facility, and conventional thermal unit integrated with demand response programs, have been studied by [10]. The main objective of the proposed method is to minimize the total operation cost, as well as flexibility improvement. The energy and exergy analysis of integrated CAES, gas turbines, and solar dish collector to evaluate the optimal system operation under multiple conditions was developed by [11]. In [12], a new hybrid power plant, including wind turbines, CAES, and recompression-absorption refrigeration system, was proposed. Authors of [13] investigated the operation and design of a CAES system for wind power generation integration through process simulation at design and off-design conditions. In [14], scheduling of CAES integrated with energy hubs in the presence of demand response was proposed.

As previously discussed, the operation and efficiency of a CAES facility are highly dependent on thermodynamic characteristics. However, our review shows that there have been very few attempts made to involve thermodynamic conditions in CAES scheduling. CAES facility is expressed based on its energy ratio and heat rate [15, 16]. The amount of electricity consumed by the compressor per unit of energy generated by the expander expresses the energy ratio. The amount of fuel burned per unit of generated power by the turbine expresses the heat rate. The energy ratio is a function of current compressed air in the cavern and the value of related air from the cavern at the current time. Authors of [16] found that during charging mode, the cavern input air flow rate depends on a cavern state of charge (SoC). Furthermore, during discharging, the cavern output airflow rate would be different for various levels of discharge. Therefore, for more realistic scheduling and better-managed operating expenditure of the CAES facility, all thermodynamic limitations for different conditions must be considered in an integrated model. In addition to multiple advantages of the CAES facility, greenhouse gas emission is its main drawback. Hence, in [17], the post-combusting carbon capture is extended to reduce greenhouse gas emissions from CAES. In [15], a self-scheduling of the CAES facility to participate in energy, spinning, and non-spinning reserve by considering the thermodynamic characteristics was studied. In this study, the CAES facility was recognized as a privately-owned merchant unit, but the co-operation of the facility with renewable energy was not considered. In [18], the performance assessment of a combined heat and CAES technology based on the thermodynamic analysis was studied. Also, the effect of electrical hating and power distribution ratio was evaluated in this work. Authors of [19] proposed a thermodynamic analysis of the hybrid solar/wind and CAES system by implemented roadways of abandoned coal mines as compressed air storage space. In [20], investigated a new high-temperature hybrid CAES system. A thermodynamic analysis of the proposed system is presented considering parametric studies. This paper illustrates that the temperature and operation pressure of thermal energy storage has a significant impact on CAES performance. The authors of [21] stated that the current large-scale CAES facility is limited by the underground

exploration and inherent risks. Therefore, a mini-CAES concept where the cavity is shallower than the current CAES facility is investigated. Numerical results release the effectiveness of the mini-CAES facility for the integration of renewable energy compared to the deeper CAES. Optimum operation and off-design performance for the multistage compression in adiabatic CAES was developed by [22].

Apart from thermodynamic conditions, the participation of the CAES facility in energy markets has not been much addressed in the literature. In [23], a reserve capacity model for advanced adiabatic CAES considering the air pressure, thermal storage, and power output limitations presented. The proposed model was used for analyzing the impact of CAES on reserve and energy market schedules, wind curtailment, as well as operating costs. A thermodynamic analysis of the off-design operation of a hybrid power plant with CAES and wind farm was performed by [24]. The proposed system was simulated to operate in the Italian power exchange market. The authors also investigated the island and grid-connected operations for the proposed hybrid system. Authors of [25] proposed a detailed mathematical model of adiabatic CAES facility to use for dynamic analyses and the power system steady-state. The performance of the proposed model was examined when providing frequency regulation in the test system integrated with a high penetration of wind power. In [26], a hybrid energy storage system based on integrated thermochemical and CAES facilities was developed. The proposed hybrid system can store the power from solar, wind, and off-peach electricity. The optimal participation of small-scale CAES incorporated with an electric vehicle charging station in the day-ahead wholesale market was developed by [27]. The optimal operation of underwater CAES incorporated with wind energy to participate in the spot market was studied by [28]. While the effects of an energy storage unit in the mitigating of the wind fluctuation were highlighted by the authors, the uncertainty modeling of the wind and power market has been ignored.

In addition to the thermodynamic analysis for CAES, the carbon dioxide (CO2) energy system in the field of renewable energy integration and environmental benefits is exposed by the thermodynamic condition. The energy and exergy analysis of novel CO2 energy storage coupled with ejector and

thermal energy storage was investigated by [29]. In [30], an advanced exergoeconomic assessment for supercritical CO2 storage was proposed. Results show that the exergy cost can be reduced up to 38.86% in the best condition. A novel two-stage transcortical CO2 storage system using advanced and conventional exergy analysis was studied by [31]. A review of supercritical CO2 storage for high-grade heating waste to electricity conversion was studied by [32]. In [33], techno-economic analysis for different cycles for high-temperature heat-waste to electricity conversion by CO2 was investigated. Besides the CAES, liquid air energy storage (LAES) has been attracted much attention. For example, the performance and experimental results of LAES were investigated by [34], for the first time in the word. Also, in [35], LAES coupled with bed cold thermal storage considering the thermodynamic analysis was investigated.

The literature review shows the importance of optimal scheduling of CAES as a large-scale, cost-effective, and high-efficiency technology integrated with renewable energy. However, the need for a comprehensive model considering the thermodynamic characteristics with advanced features of CAES to achieve a more realistic model in the CAES performance has remained. Furthermore, participation in multi-energy markets, such as energy and reserve markets by the CAES facility, must be done taking into account all the limitations and thermodynamic conditions.

To the best knowledge of the authors, the reviewed works have not extensively evaluated the comprehensive model of the CAES facility, considering thermodynamic characteristics for charging and discharging schemes. as well as recovery cycle capability. Furthermore, thermodynamic modeling of CAES incorporated with renewable energy as a hybrid system to participate in markets has rarely been investigated in the literature. The significant gaps in the literature re as follows:

- In [6-14], while the operation of conventional CAES in the power system from technical, economic, and environmental perspectives have been studied, the thermodynamic model of CAES with recovery capability to participate in the energy market has been ignored.

- In [15-22], although the thermodynamic assessment of CAES and adiabatic CAES have been investigated, the operation of CAES incorporated with large-scale wind and solar farms to participate in energy markets has been ignored. Also, the recovery cycle as a suitable heating source has not been considered in these works.
- In [23-28], while the application of the CAES facility in energy markets was studied, the thermodynamic characteristics of CAES in optimal operation that highly expose the CAES performance have been ignored. Also, the optimal charging and discharging mode of CAES integrated with renewable energy based on the thermodynamic modeling not considered in this researches.
- In [29-35], while the thermodynamic analysis of CAES, LAES, and CO2 based energy storage system has been investigated by the authors, the performance of these technologies in the hybrid system considering the power market not considered.

Therefore, to cover the mentioned gaps, this work presents a new optimal scheduling framework for a developed CAES facility coupled with wind/PV farms and thermal units to participate in the energy and reserve market, considering the thermodynamic characteristics. Unlike the traditional CAES models, in an advanced CAES, the output turbine airflow, which has a high temperature and is usually wasted from the exhaust, is restored as a recovery mode. The recovery heat from the turbine is used in the preheater to increase the temperature of cavern output airflow during discharging. In this way, while increasing the turbine efficiency, the need for external fuel for the combustion of air is significantly reduced. The main contribution of the paper includes the development of a realistic model for the hybrid thermal, wind/PV farm with a developed CAES in the presence of thermodynamic characteristics. However, the proposed hybrid system can facilitate the integration of renewable energy as well as thermal unit operation through proper charging and discharging management. Considering the recovery cycle capability for the CAES facility will have significant effects on the operation cost. The main contributions of this paper can be summarized as follows:

- Proposing hybrid wind and solar farms, thermal units, and advanced CAES considering thermodynamic conditions, including cavern pressure, import/export airflow rate, compressor, and turbine efficiency.
- Analyzing the CAES facility operation during charging, discharging modes, simultaneously, and calculating cavern SoC-based thermodynamic characteristics.
- Proposing the optimal bidding strategy for the hybrid system to participate in energy and reserve markets.
- Considering the recovery cycle for the CAES as a suitable and cost-effective resource which reduces the required fuel in the combustion, consequently operation cost.
- Proposing the scenario-based stochastic approach to address the high-level uncertainties, including energy and reserve markets price, wind, and PV power output.

The organization of this paper is as follows. Section II provides the formulation of hybrid system formulation, including objective function and related constraints. Section III describes the methodology, including the thermodynamic conditions and analysis, the recovery cycle as part of the advanced CAES operation, and uncertainty modeling for wind and PV farms' power output, as well as energy prices. Section IV presents numerical results and investigates the performance of the proposed scheduling. Finally, Section V concludes the paper.

II. System description

In this section, the scheduling model of the hybrid thermal, wind/PV, and a developed CAES facility to participate in energy and reserve markets is presented. Figure 1 depicts a common schematic of the CAES, which consists of two high and low compressors and turbines with a cavern. During charging, surplus power is given to the motor, which helps compressors to store the high-pressure air into the cavern that is located under-ground. During discharging times, the high-pressure air is released from

the cavern and is heated in the combustor using the external fuel (like natural gas) then used two turbines to generate electricity.

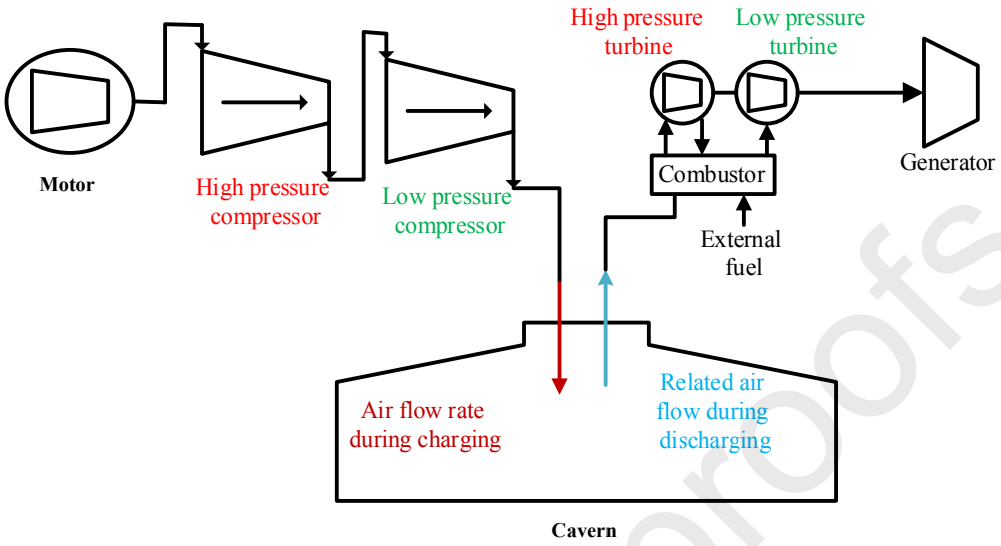

Figure. 1. The schematic of a conventional CAES facility

Figure 2 shows the proposed hybrid system, which consists of thermal generators, wind, and PV farms, as well as a CAES facility. Thermal units and wind/PV farms can participate in energy and reserve markets independently. However, the CAES compressors, by using surplus power and/or purchasing power from the market, can store air in the cavern during off-peak times. At on-peak times, when the system has to generate a high value of electricity, the CAES facility releases the high-pressure air to generate power.

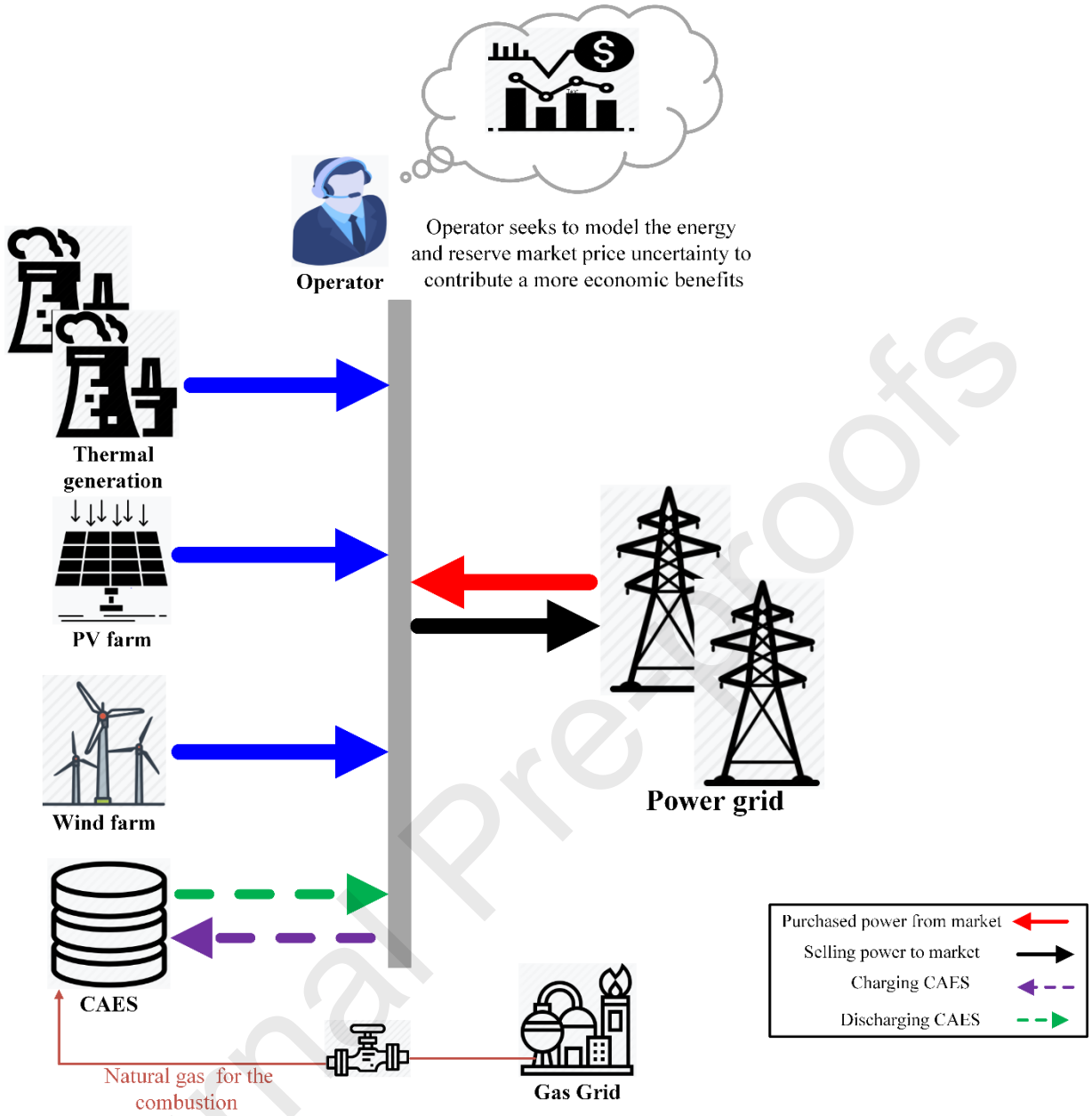

Figure. 2. The structure of the proposed hybrid thermal, wind/ PV, and a developed CAES facility

A. Objective function

The main objective of the model is to maximize the total profit of the hybrid system through participation in the energy and reserve markets. However, to take the uncertainty of generated power by renewable energy resources into account, uncertainty modeling via a scenario-based stochastic approach is implemented. To model the price (energy and reserve prices) and RES power output uncertainties, a large number of scenarios are generated. Then, as explained in reference [36], the expected value for profit is calculated. The objective function can be formulated as follows:

$$Max\ \ Z = \sum_{\omega=1}^{N_\omega} \rho_\omega \left[\sum_{t}^{NT} \left(\begin{array}{l} \pi_{t,\omega}^{e} \left(\sum_{G}^{NG} P_{G,t,\omega} + P_{w,t,\omega} + P_{pv,t,\omega} + P_{t,\omega}^{d} - P_{t,\omega}^{c} \right) + \\ \pi_{t,\omega}^{e,r} \left(\sum_{G \in N_G} P_{G,t,\omega}^{r} + P_{w,t,\omega}^{r} + P_{pv,t,\omega}^{r} + P_{t,\omega}^{d,r} \right) - \\ \left[(P_{t,\omega}^{d} + P_{t,\omega}^{d,r}) \times (HR^{nom} \times \pi^{NG} + VOM^{\exp}) + P_{t,\omega}^{c} \times VOM^{c} \right] \\ -\sum_{G}^{NG} F(P_{G,t,\omega}) - C_{pv}^{curt} P_{pv,t,\omega}^{curt} - C_{w}^{curt} P_{w,t,\omega}^{curt} \end{array} \right) \right] \quad (1)$$

According to (1), the objective function consists of multiple terms for both energy and reserve markets. The term within the first parentheses represents the revenue of the hybrid system obtained from selling power to the energy market, including selling power from the thermal units, wind and PV farms, as well as the power output of CAES facility during discharge mode minus power purchased from the market during charging mode. In the same way, the revenue of selling power to the reserve market is represented by the second term of the objective function (1). The operating cost of the CAES facility during discharging, including variable operation cost, as well as the cost of burning natural gas during the generation of P_t^d and $P_t^{d,r}$ to generate power for energy and reserve market applications, is expressed by the third line of the objective function (1). The heat rate effect on discharging mode will be described in future sections. The fourth term in (1) represents the variable operating cost during the charging mode. The fifth term of the objective function (1) represents the operation cost of thermal units, including start-up/shut-down and generation costs. The generation cost of thermal units is similarly approximated by a piecewise-linear model that it was used in [37]. The power curtailment costs for PV and wind farms are represented in the two last terms of (1). In the objective function (1), ρ_ω represents the probability of ω^{th} scenario.

B. Problem constraints

There are multiple constraints for the proposed scheduling model of the hybrid system, which are described in the following:

- *Thermal unit constraints:*

The power generation of thermal G unit at time t is limited by the minimum and maximum value of power generation as in (2). Equations (3) and (4) show the ramp-up and ramp-down constraints. The thermal unit G must be on/off for a minimum time before it can be shut down or restarted, respectively. The minimum up and down time limits for the thermal generation unit is given by (5)-(8), respectively [38]. The constraints in (9) -(12) are related to the start-up and shut-down costs limitation, respectively.

$$P_G^{\min} . I_{G,t,\omega} \le P_{G,t,\omega} \le P_G^{\max} . I_{G,t,\omega} \tag{2}$$

$$P_{G,t,\omega} - P_{G,t-1,\omega} \le UR_G \tag{3}$$

$$P_{G,t-1,\omega} - P_{G,t,\omega} \le UD_G \tag{4}$$

$$I_{G,t,\omega} - I_{G,t-1,\omega} \le I_{G,t+TU_{G,u}} \tag{5}$$

$$TU_{G,u} = \begin{cases} u & u \le MUT_G \\ 0 & u > MUT_G \end{cases} \tag{6}$$

$$I_{G,t-1,\omega} - I_{G,t,\omega} \le 1 - I_{G,t+TD_{G,u}} \tag{7}$$

$$TD_{G,u} = \begin{cases} u & u \le MDT_G \\ 0 & u > MDT_G \end{cases} \tag{8}$$

$$SU_{G,t,\omega} \ge SUC_G (I_{G,t,\omega} - I_{G,t-1,\omega}) \tag{9}$$

$$SU_{G,t,\omega} \ge 0 \tag{10}$$

$$SD_{G,t,\omega} \ge SDC_G (I_{G,t-1,\omega} - I_{G,t,\omega}) \tag{11}$$

$$SD_{G,t,\omega} \ge 0 \tag{12}$$

- *CAES constraints:*

The limitations of charging and discharging power are given in (13) and (14), respectively. Constraint (15) represents that the CAES operates in only one mode (charging or discharging) at each period. Due to the participation in both energy and reserve markets, there are different restrictions on the cavern capacity. However, to provide the required power to participate in both energy and reserve markets, the cavern should have a sufficient capacity. Therefore, the cavern capacity should not be less than $SoC_{\min}$ as given in (16). It should be noted that, when the CAES facility operates in discharging mode, the cavern SoC is a function of an energy ratio [15]. To follow the charge schedule, the maximum cavern capacity

should not be more than $SoC_{\max}$ that is represented in (17). Constraint (18) shows the value of cavern SoC in time *t* that is equal to the sum of time *t-1* SoC and the amount of energy that is imported/exported during the charging/discharging mode at the time *t*.

$$P^{c}_{\min} x^{c}_{t,\omega} \le P^{c}_{t,\omega} \le P^{c}_{\max} x^{c}_{t,\omega} \tag{13}$$

$$P^{d,\exp}_{\min} x^{d}_{t,\omega} \le P^{d}_{t,\omega} + P^{d,r}_{t,\omega} \le P^{d,\exp}_{\max} x^{d}_{t,\omega} \tag{14}$$

$$x^{c}_{t,\omega} + x^{d}_{t,\omega} \le 1 \tag{15}$$

$$SoC_{\min} \le SoC_{t,\omega} - \frac{\left(P^{d}_{t,\omega} + P^{d,r}_{t,\omega}\right) \times ER}{E_{\max}} \tag{16}$$

$$SoC_{t,\omega} + \frac{P^{c}_{t,\omega}}{E_{\max}} \le SoC_{\max} \tag{17}$$

$$SoC_{t,\omega} = SoC_{t-1,\omega} - \frac{\left\{P^{d}_{t,\omega} + P^{d,r}_{t,\omega}\right\} \times ER}{E_{\max}} + \frac{P^{c}_{t,\omega}}{E_{\max}} \tag{18}$$

However, the energy capacity constraint of the CAES facility is a function of thermodynamic characteristics such as cavern pressure, import/export airflow rate, compressor and turbine efficiency, etc. Therefore, we will represent the energy capacity constraints considering thermodynamic characteristics in the following section.

III. Methodology

The operation of the CAES facility is a function of multiple thermodynamic conditions. Therefore, all the energy capacity equations must be represented considering these conditions. In both the operational modes (i.e., charging and discharging), the cavern SoC depends on several parameters like pressure, efficiency, and airflow rate. However, to follow the charge schedule and required airflow rate during discharging, the thermodynamic parameters should be taken into account. For this purpose, the effect of SoC for both charging and discharging modes is analyzed separately.

A) SoC analysis in the charging process

In references [15, 16] the variation of airflow rate and consumption power by the compressor for different charging levels when the cavern is fully charged is investigated. However, the variation of pressure during the charge level is neglected. The cavern pressure is an important parameter affecting the rate of injection air during charging. We added the pressure variation during the full charge process to the previous investigations, which is depicted in Figure 3.

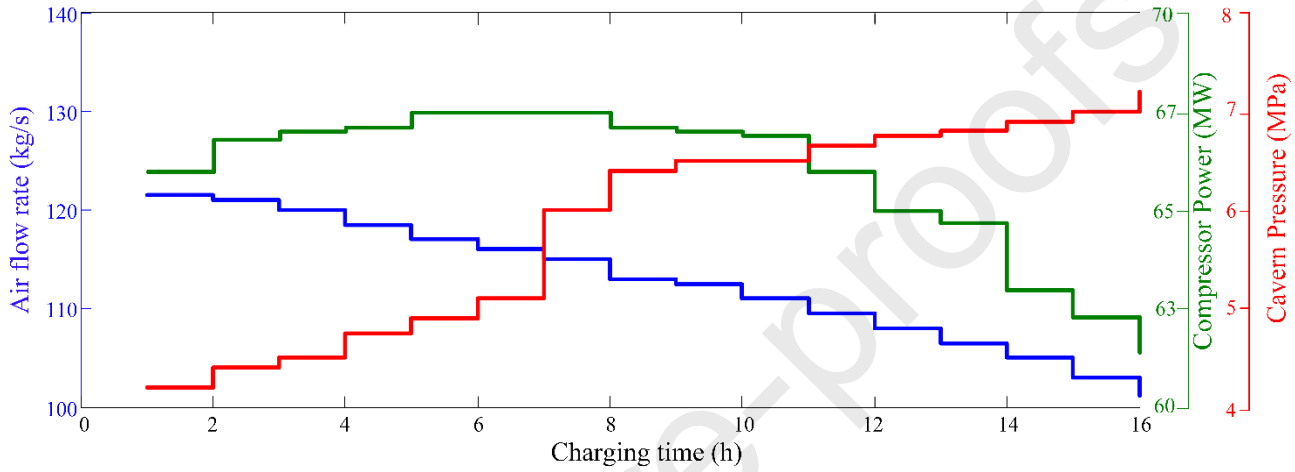

Figure. 3. The variation of airflow rate, compressor power, cavern pressure during the different charging time

As can be seen from Figure 3, when the compressor charges the cavern more times, the cavern pressure increases. By this action, the more air is stored in the cavern. The massive air volume in the cavern does not allow the input airflow rate to be high. Therefore, the airflow rate, and consequently, the compressor power decrease.

Due to the variation of pressure, airflow rate, and compressor power, the charging process causes that the cavern SoC not to be constant. As stated in [15, 16], when the compressor operates with P_t^c at time *t*, the mass of stored air in the cavern depends on current SoC and P_t^c . This can be presented by a function as follows:

$$\text{Mass of stored air} \propto \Re(SoC_{t,\omega}, P_{t,\omega}^c) \tag{19}$$

The current SoC value, formulated in (16), can be represented as follows:

$$SoC_{t,\omega} = SoC_{t-1,\omega} - \Gamma(P_{t,\omega}^d) + \Psi(P_{t,\omega}^c) \tag{20}$$

where $\Gamma(P^d_{t,\omega})$ and $\Psi(P^c_{t,\omega})$ are discharging and charging functions, respectively, which determine the variation of air mass at time *t*. $\Gamma(P^d_{t,\omega})$ will be described in later sections. However, based on the above description about the effect of level charging on SoC, $\Psi(P^c_{t,\omega})$ can be formulated as follows:

$$\Psi(P^c_{t,\omega}) = \frac{\Re(SoC_{t,\omega},\ P^c_{t,\omega})}{AM^{\max}} \tag{21}$$

where $AM^{\max}$ is the maximum mass of air in the cavern in *kg*.

According to Figure 3, we define a new parameter named airflow rate during charging (AF^c), which is obtained by dividing the airflow rate by the power consumption of the compressor and cavern pressure. It should be noted that AF^c is different from AFR^c that is presented in [15]. The cavern SoC at time *t* can be calculated by accumulating the mass of air up to time t. According to Figure 3, the amount of stored air during full charging is 6.58 million *kg*. The total mass of compressed air in the cavern is reported to be 9.48 million *kg* [16]. Therefore, it can be determined that the minimum mass of air that should be remained in the cavern is 2.9 million *kg*. Thus, $SoC_{\min}$ will be 31 %. In this way, we can depict AF^c versus SoC, which is shown in Figure 4. As can be seen, as the level of SoC (cumulative mass of air up to time t) increases, AF^c decreases. This is because, in the high-pressure, the high-level of air could not be saved in the cavern.

Based on the above discussion, the function $\Re$ can be formulated as follows:

$$\Re(SoC_{t,\omega},\ P^c_{t,\omega}) = P^c_{t,\omega} \times Pa_{c,t} \times AF^c(SoC_{t,\omega}) \times 3600 \tag{22}$$

B) SoC analysis in the discharging process

The related airflow rate of the CAES facility during discharging depends on a power generation level. For high-level power generation, the airflow rate is required to be high and vice versa. In [9, 16], the variation of air flow rate for different generation level is analyzed. However, the turbine inlet pressure as an important parameter affecting the turbine operation is neglected. Thus, we depicted the airflow rate and turbine inlet pressure per level of power generation that is shown in Figure. 5. As can be seen, as the level of power generation increases, the airflow rate and turbine inlet pressure increase.

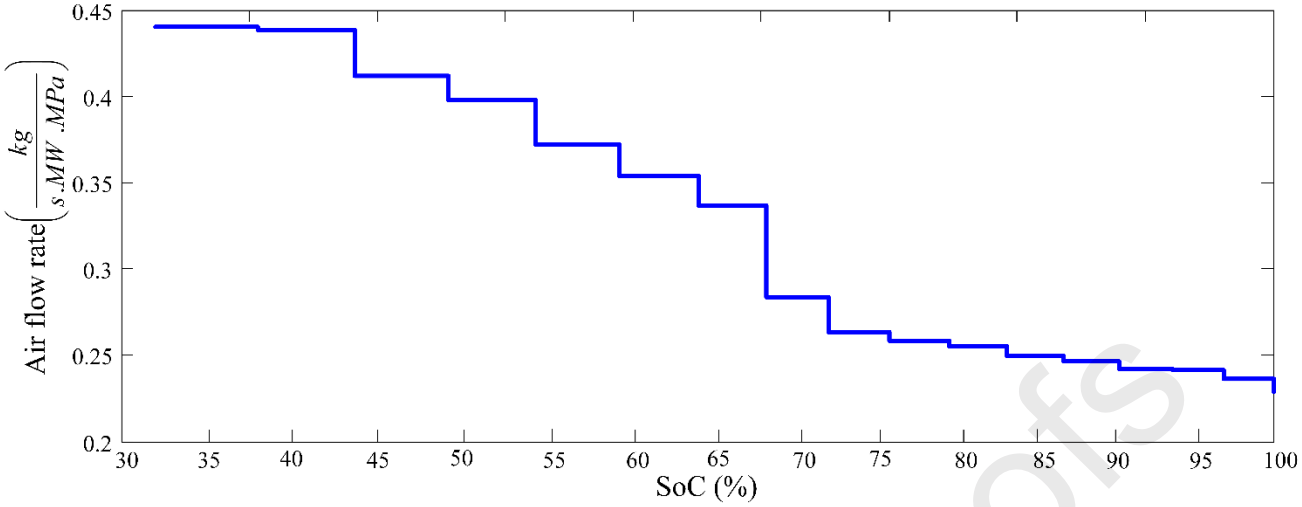

Figure. 4. Airflow rate versus cavern SoC during charging mode

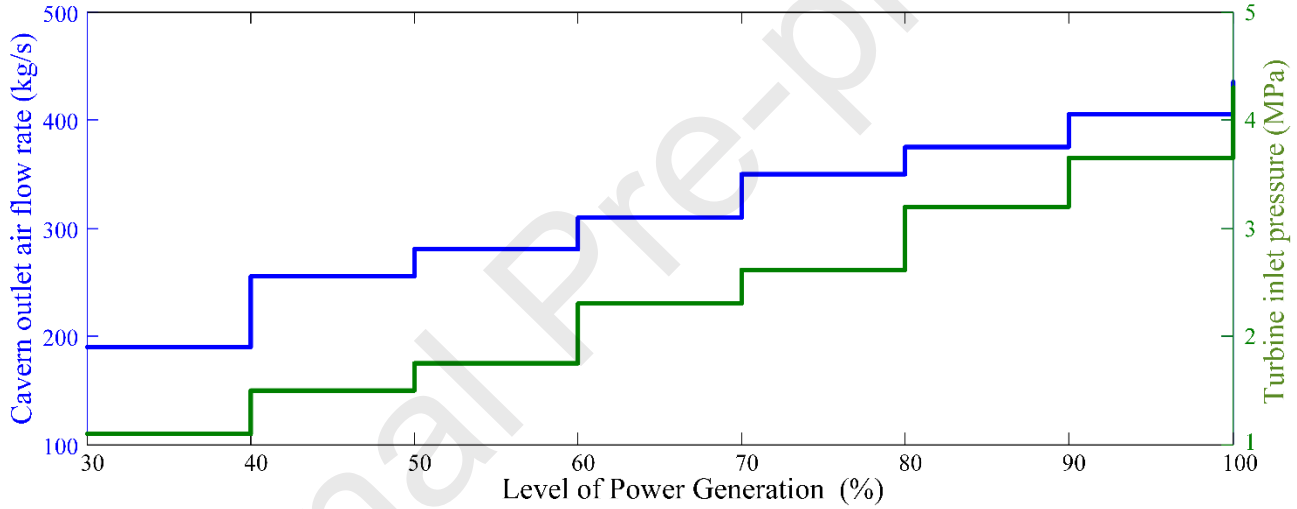

Figure. 5. The variation of airflow rate and turbine inlet pressure during the discharge process

By dividing the related airflow rate from the cavern by the power generation for different levels and turbine inlet pressure, a new parameter named AF^d (airflow rate during the discharging process) is calculated. Therefore, AF^d per unit of power generation is calculated, which is shown in Figure 6. For a lower generation of electricity, the required AF^d is 5.72 $Kg/MW.s.MPa$. However, for full level power generation, AF^d is 1.25 $Kg/MW.s.MPa$. It is shown that during the discharge process, the cavern SoC is not constant and relies on the level of power generation. It should be noted that the turbine efficiency effects justify the behavior of Figure. 6 [16].

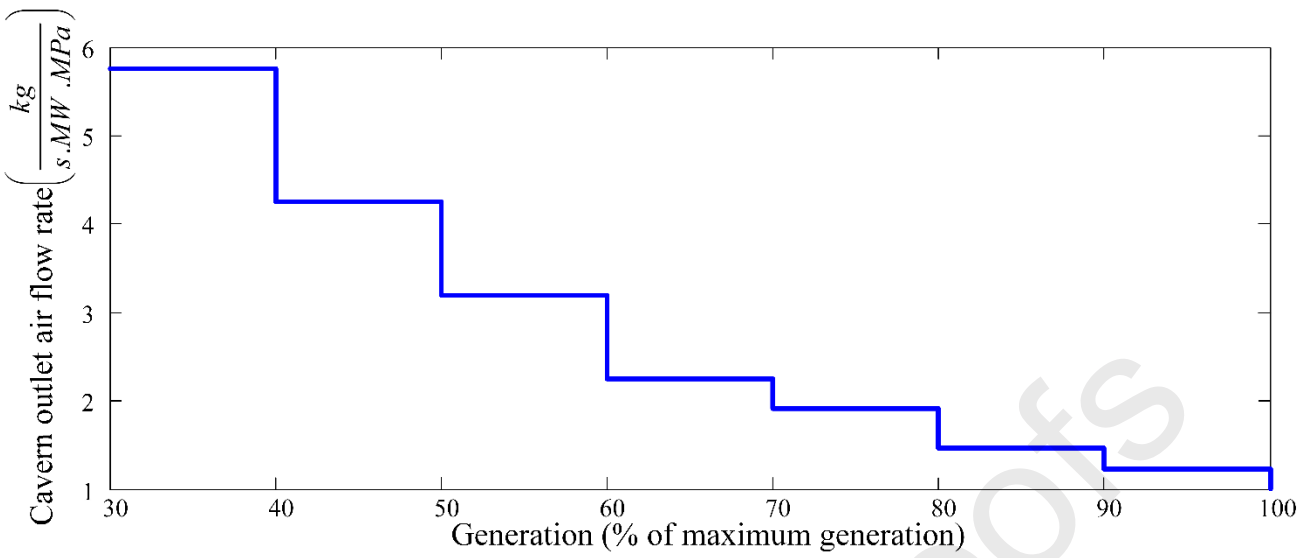

Figure. 6. Airflow rate versus the power generation level during the discharge process

According to Figures 5 and 6, the related mass of air from the cavern during discharging for different levels of generation is not constant and should be considered in CAES scheduling. Therefore, the total related mass of air to combustor at time *t* to generate P_t^d is: $P_t^d \times Pa_{d,t} \times AF^d(P_t^d) \times 3600$. Thus, $\Gamma(P_t^d)$ can be formulated as follows:

$$\Gamma(P_{t,\omega}^d) = \frac{P_{t,\omega}^d \times Pa_{d,t} \times AF^d(P_{t,\omega}^d) \times 3600}{AM^{\max}} \tag{23}$$

According to Equations (18) and (19), Equation (16) can be rewritten as follows:

$$SoC_{t,\omega} = SoC_{t-1,\omega} - \frac{P_{t,\omega}^d \times Pa_{d,t} \times AF^d(P_{t,\omega}^d) \times 3600}{AM^{\max}} + \frac{P_{t,\omega}^c \times Pa_{c,t} \times AF^c(SoC_{t,\omega}) \times 3600}{AM^{\max}} \tag{24}$$

- *Heat rate function*

As mentioned in the previous section, the heat rate (HR) shows the ratio of fuel burned per unit of generated power by the turbine. Therefore, in discharging mode, HR is a function of power generation levels [15]. Based on data provided in [16], the variation of HR is depicted for different levels of the generation, which is shown in Figure 7. As can be seen, as the level of power generation decreases HR increases. The main reason for this phenomenon is the turbine efficiency. The efficiency of the turbine in lower levels of generation decreases, thus it increases the airflow rate, and subsequently, a larger

amount of fuel must be burned to generate the electricity. In higher levels of power generation, turbine efficiency increases, and subsequently, HR decreases (see Figure 7).

According to Figure 7, we can reformulate the operation cost of natural gas that represented in the third term of (1) as follows:

$$\text{Cost of natural gas: } P^{d}_{t,\omega} \times HR\,(P^{d}_{t,\omega}) \times \pi^{NG} \tag{25}$$

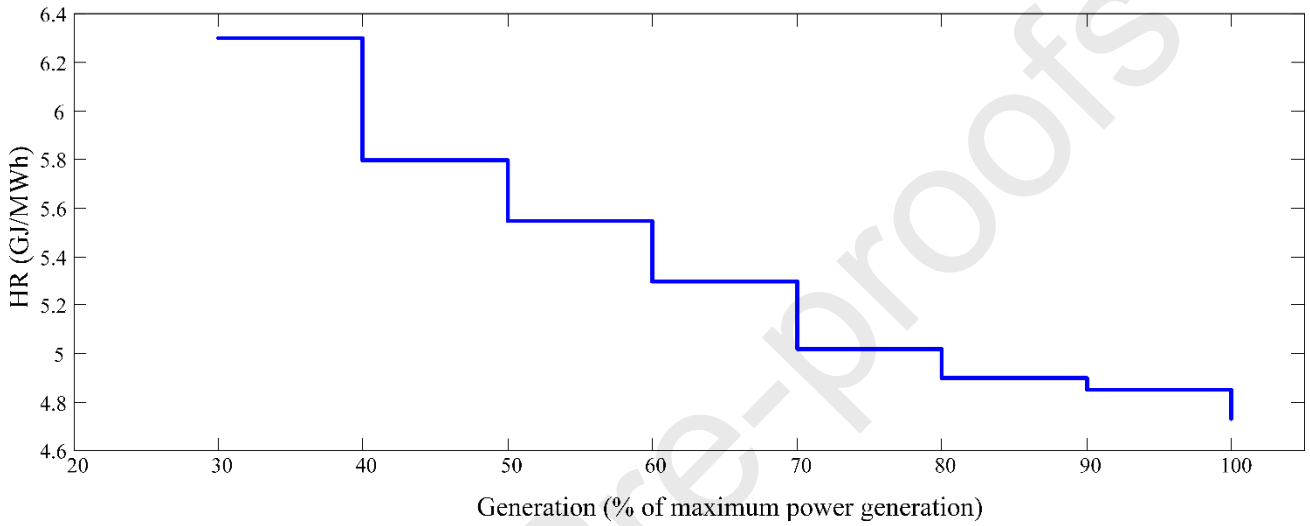

Figure. 7. The HR variation for different levels of generation [16]

C) Recovery cycle

To increase the turbine efficiency and reduce fuel rejection for combustion, the turbine's exhaust gas, usually at a higher temperature, is used as an energy source. Authors of [39] concluded that if the generated heat during air compression is not utilized, the process efficiency will be low and additional heat is required during the expansion process. The turbine is composed of two main components: expander and burner. Figure 8 shows the part of the CAES facility structure, consisting of an expander, burner, and recuperator, which enable the recovery cycle.

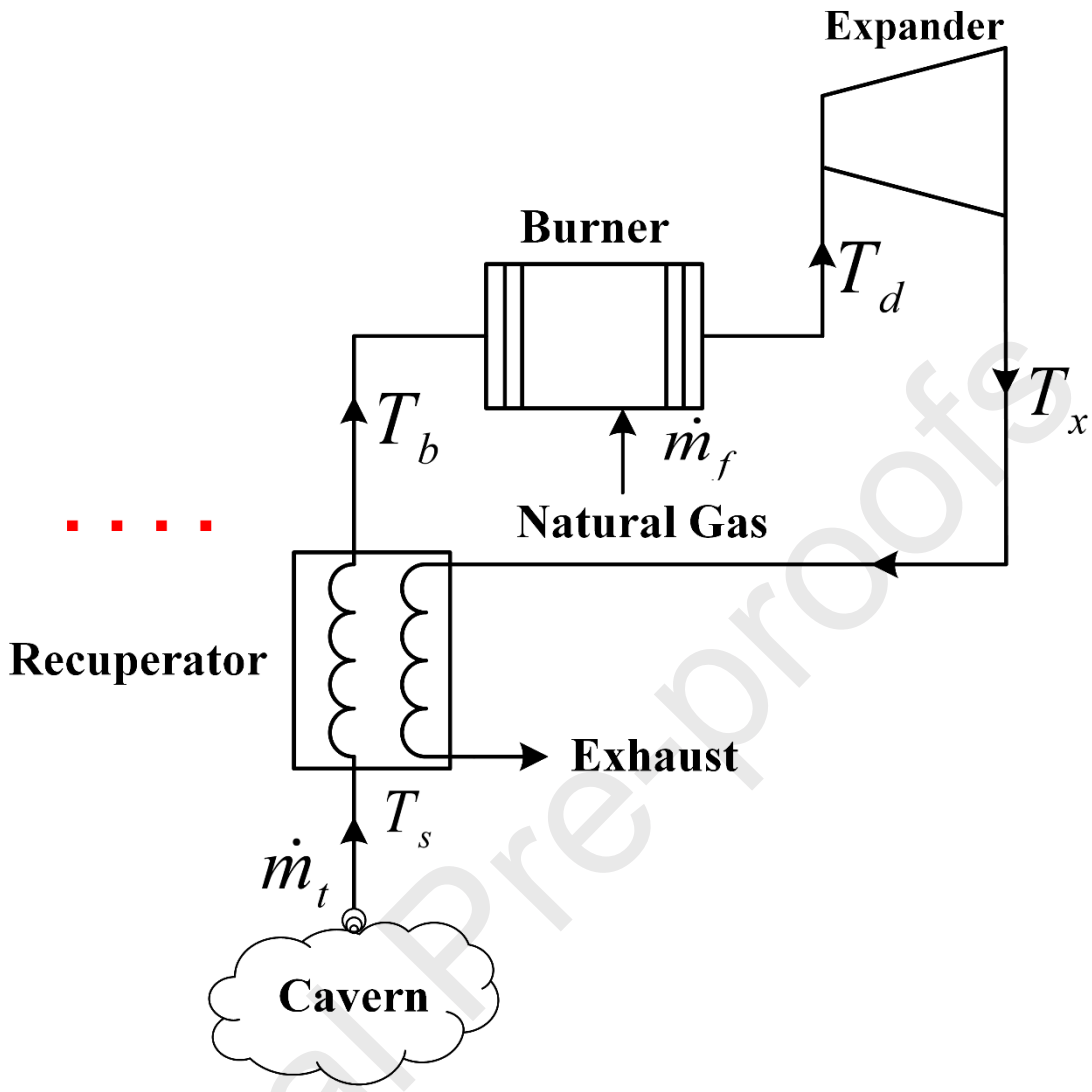

Figure. 8. The part of the CAES facility that enables the recovery cycle

The released air from the cavern that is low temperature needs to reach the ideal temperature for combustion. Before injecting the external fuel into the combustion chamber, the released air is heated by passing through the recuperator. The released air from the cavern feeds the recuperator cold side at a temperature T_s while its hot side is fed by the exhaust gas at temperature T_x , in the end, the outlet air of the recuperator at temperature T_b is released. This temperature is unknown. The heat exchange process can be described by its efficacy [25], which is defined as the ratio of actual reformed head transfer to the maximum possible heat transfer. Thus, we have:

$$\varepsilon_r = \frac{q_0}{q_0^{\max}} \tag{26}$$

It can be said that the inlet temperature of the burner (T_b) does not change immediately, therefore is calculated by [25]:

$$\bar{T_b} = \frac{T_s}{T_{b_0}} + u_r \tag{27}$$

$$\dot{u_r} = \frac{1}{\tau_R}\left[\varepsilon_r\left(\frac{\bar{T_x}T_{x_0} - T_s}{T_{b_0}}\right) - u_r\right] \tag{28}$$

where u_r is the heated dynamic added by the recuperator. By solving the Equations (27) and (28), $\bar{T}_{b_0}$ is calculated. For steady-state conditions, we have $\bar{T_x} = 1$ and $\bar{T_b} = 1$. After that, the heated air at the temperature T_b enters the combustion chamber. Combustion occurs by the amalgamation of air and fuel. The temperature outlet air of the burner at temperature T_d arises as $\dot{m}_f$ (the value of injection fuel) increases while it cools down as the released air from the cavern increases. T_d can be formulated as:

$$T_d = \bar{T_b}\left(\frac{T_{b_0}}{T_{d_0}}\right) + \frac{T_{d_0} - T_{b_0}}{T_{d_0}}\left(\frac{\bar{\dot{m}}_f}{\bar{\dot{m}}_t}\right) \tag{29}$$

For isotropic air combustion in the expander, the exhaust air at temperature T_x is a function of inlet air at temperature T_d, and the pressure ratio Ω_t as follows:

$$\Omega_t^{-\frac{\gamma-1}{\gamma}} = \frac{T_x}{T_d} \tag{30}$$

where γ is the heat capacity ratio [25]. According to (30), and assuming that the actual pressure ratio of the turbine is approximately equal to the nominal value [16], the outlet air temperature of the expander in p.u. is calculated by:

$$\bar{T_x} = \frac{T_d T_{d_0}}{T_x}\left\{1 - \left[1 - \frac{1}{\left(\Omega_t \bar{\dot{m}}_t\right)^{\frac{\gamma-1}{\gamma}}}\right]\right\} \tag{31}$$

By finding T_x , the amount of heat energy that is added to the released air will be calculated. Approximately, the power output of expander in p.u. to the total rated power of turbine can be calculated as:

$$P_{t,\omega} = \frac{\eta_t c_p \bar{\dot{m}}_{t_0}}{10^3 P_{t_0}} \bar{\dot{m}}_{t,\omega} \left(T_{d_0} \bar{T}_d - T_{x_0} \bar{T}_x \right) \tag{32}$$

It can be seen that for a certain mass of fuel, as T_x increases, the power output will increase. In other words, adding the recovery cycle to the CAES facility will reduce HR. This has a significant impact on system cost. In the results section (section V), the operation of the CAES facility with and without the recovery cycle will be analyzed.

- *Uncertainty Modeling*

The power generated by wind and PV farms is subjected to the uncertainty related to wind speed and irradiation, respectively. The probabilistic nature of renewable energy, as well as price uncertainty, exposed the optimal operation of the hybrid system. As previously discussed, wind and PV farms' power, as well as energy and reserve prices are captured based on a scenario-based stochastic approach. Each random variable is subjected to a corresponding distribution function, which is described in the following.

- *Wind farm power output*

Studies show that the probability distribution of generated power by the wind farm is varied with the real power output by it [40]. Based on the real power output and forecast values of Khaf station that contains 66 wind turbines in Iran, between 2015 and 2016 [41], a model of the probability distribution for the generated power by wind farm was set up by fitting the Weibull distribution. There are three main steps to achieve this goal:

1. The forecasting data at each period were normalized in ascending order;
2. The series of data obtained in the first step is divided into 100 groups. There is 0.01 p.u. the power difference between all contiguous groups;

3. Based on the obtained groups in the previous step, the corresponding data were fitted to the Weibull probability distribution function, which is given by (33):

$$f\ (\mathrm{V}) = \frac{r}{c}\left(\frac{V}{c}\right)^{r-1} \exp\left[-\left(\frac{V}{c}\right)^{r}\right] \tag{33}$$

where *r* and *c* describe the parameters related to the Weibull distribution that can be estimated by the maximum likelihood (ML) technique [42]. Therefore, based on the forecasted wind speed, by using the above steps, the Weibull PDF is calculated. After that, the wind speed is converted into power based on (34). Constraint (35) limits the value of the wind power curtailment at each period.

$$P_{w,t,\omega} = \begin{cases} 0 & 0 \le V \le V_{cut-in} \\ (k_1 + k_2 V_{t,\omega} + k_3 V_{t,\omega}^2) P_{w_{rated}} & V_{cut-in} \le V \le V_{rated} \\ P_{W_{rated}} & V_{rated} \le V \le V_{cut-out} \\ 0 & V_{cut-out} \le V \end{cases} \tag{34}$$

$$P_{w,t,\omega}^{curt} \le P_{w,t,\omega} \tag{35}$$

Based on the real power generated in different stations, especially the KHAF station, it is obvious that there is a provisional correlation between real data. To verify the authenticity of simulations based on the forecasting data, the correlation model for the power generation of a wind farm should be considered. All the steps of the correlation model are described in [43].

- *PV farm power output*

The power generation of PV farms depends on irradiation and air temperature. Based on the estimated data, assumed that the PV farm contains different PV panels is embedded in the KHAF station. Hence, the probability distribution function related to PV power generation is set up by fitting the Normal distribution, which its PDF is defined as:

$$f\ (P_{pv}) = \frac{1}{\sqrt{2\pi}\times\sigma}\exp\left(-\frac{((P_{pv})-\mu)^2}{2\times\sigma^2}\right) \tag{36}$$

All the steps with data fitting, which are presented for the power generated by wind farms, are established for the PV farm [43]. The parameters of the Normal distribution are obtained by the

maximum likelihood estimation approach. After that, using (37), the generated power by PV farm is calculated. Constraint (38) limits the value of the PV power curtailment at each period.

$$P_{pv,t,\omega} = P_{STC} \times \frac{G_{ING}}{G_{STC}} \times \left(1 + K^{'}(T_c - T_r)\right) \tag{37}$$

$$P_{pv,t,\omega}^{curt} \leq P_{pv,t,\omega} \tag{38}$$

- *Energy and reserve prices uncertainty*

The bidding strategy of hybrid wind, PV, thermal units, and developed CAES to participate in both energy and reserve markets is exposed by price uncertainty. To model hourly energy and reserve prices, a scenario-based stochastic approach is used. The probability distribution function related to energy and reserve prices is set up by fitting the Normal distribution which as (36), which is reformulated as follows:

$$f(\pi^e) = \frac{1}{\sqrt{2\pi} \times \sigma} \exp\left(-\frac{((\pi^e) - \mu_{\pi^e})^2}{2 \times \sigma_{\pi^e}^2}\right) \tag{39}$$

Based on the proposed methodology, including thermodynamic analysis, recovery cycle, and uncertainty modeling, the overall schematic of the MINLP model to solve the problem can be represented in the flowchart as depicted in Figure 9.

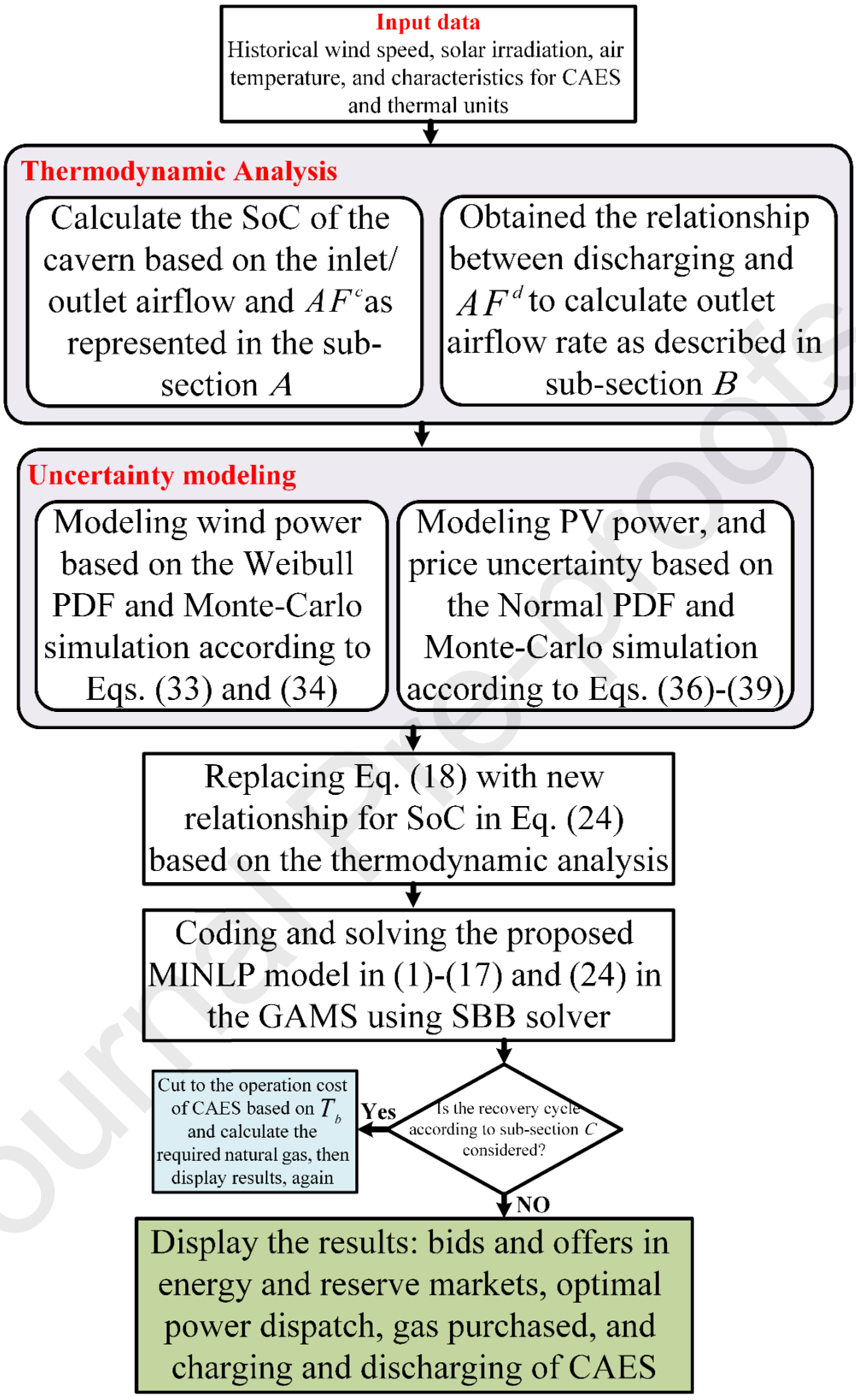

Figure. 9. Overall schematic of the proposed methodology

IV. Results and discussion

The proposed hybrid system, including CAES, Wind, PV, and thermal plants considering thermodynamic characteristics of the CAES facility, was tested on the test system. The characteristics of the hybrid system are characterized in Table I. Also, thermal units and CAES facility characteristics are given in Table II and III, respectively. To handle system uncertainty, 1000 scenarios are generated for wind and PV power output, as well as energy and reserve prices, which are reduced to 10 appropriate scenarios via the SCENRED tool in GAMS software. The forecasting error of PV, energy, and reserve price are subjected to Normal distribution with zero mean and 10% standard deviation. The forecasting error of wind power output is subjected to the Weibull distribution with characteristics in [44]. The forecasted energy and reserve markets prices are shown in Figure 10. Based on the actual data for PV and wind farms presented in section IV, the power output of PV and wind farms are depicted in Figure 11. The price of natural gas for all day is fixed and equals 20.8 $/MWh [45].

Table I. The characteristics of the hybrid system

Unit	Rated power
CAES facility	100 MW of discharging
Wind farm	50 MW
PV farm	50 MW
Thermal	6 units with different characteristics

Table I. The characteristics of 6 thermal units

	Unit 1	Unit 2	Unit 3	Unit 4	Unit 5	Unit 6
Min/ max power (MW)	75/150	75/150	50/100	30/60	50/100	30/60
$a(\$/MW^2h)$	0.0021	0.002	0.0041	0.0071	0.0022	0.0072
b($/MWh)	13.5	13.6	20.92	16.26	22.27	17.26
c($/h)	600	650	660	300	665	250
T^{on}/T^{off} *(h)*	5 / 5	5 / 5	3 / 3	1 / 1	3 / 3	1 / 1
Ramp rate (MW/h)	60	60	50	40	50	40

Table II. The characteristics of the CAES facility

Parameter	Value	Parameter	Value
Min/ Max charging power (MW)	10 / 60	Ω_t	10.856
Min/ Max discharging power (MW)	30 / 100	γ	1.4
$SoC_{\min}$ (%)	31	T_{x_0} (K)	762.4
$AM^{\max}$ (Mkg)	9.48	T_{d_0} (K)	1098.2
ε_r (p.u)	0.8	T_{b_0} (K)	599.15
τ_R (s)	25	c_p *(kj/kg.K)*	1.055
η_t	0.99	$\dot{m}_{t_0}$ (kg/s)	417

The proposed scheduling of hybrid CAES, Wind, PV, and thermal generation units was formulated as mixed-integer non-linear programming (MINLP), which was carried out in GAMS software and solved by SBB solver.

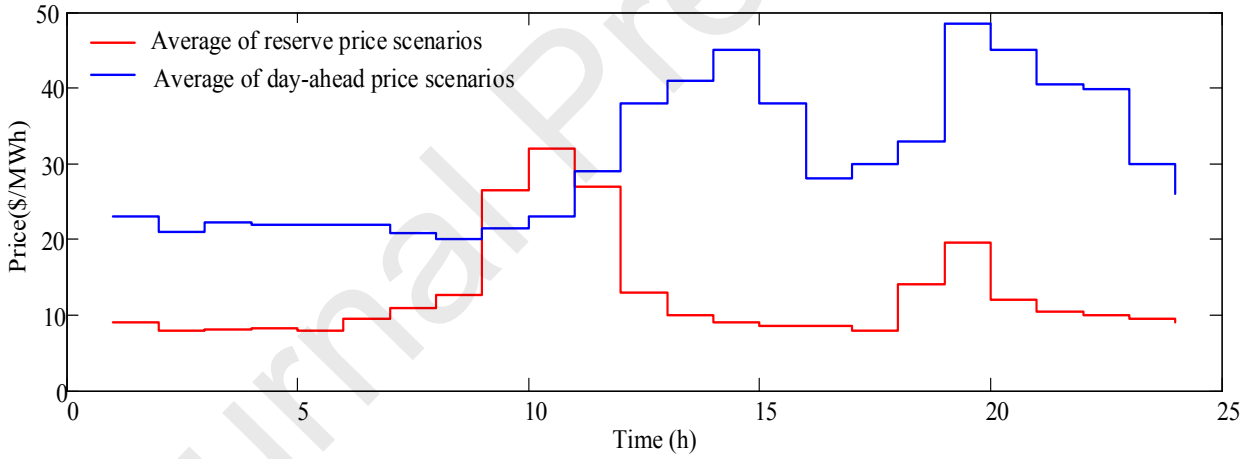

Figure. 10. The average values of energy and reserve price scenarios [15]

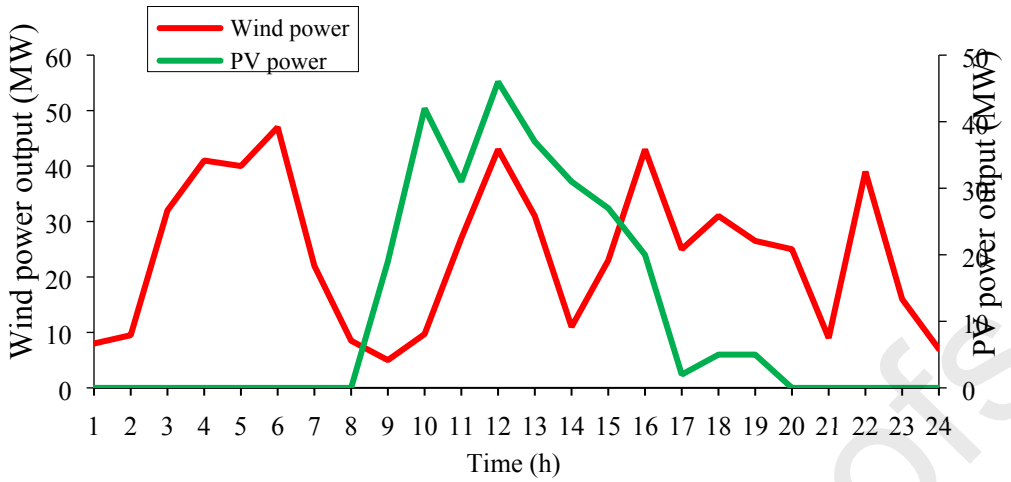

Figure. 9. Wind and PV farm power output

Simulation results are studied for the following cases:

1. Scheduling of the hybrid system without the thermodynamic characteristics and recovery cycle.
2. Scheduling of the hybrid system in the presence of the thermodynamic characteristics without the recovery cycle.
3. Scheduling of the hybrid system in the presence of both the thermodynamic characteristics and recovery cycle, simultaneously.

Table IV demonstrates the amount of profit and the corresponding probability for 10 reduced scenarios. It should be noted that scenario number 7 is chosen to analyze the details of the proposed scheduling of the hybrid system, which is described in the following.

Table IIII. The probability and corresponding profit for 10 reduced scenarios

Scenario	Probability	Profit ($)		
		Case 1	Case 2	Case 3
1	0.0602	230148.56	145843.12	194704.37
2	0.1402	169063.82	204134.94	179659.21
3	0.1322	201939.75	184729.56	185238.19
4	0.1076	189644.37	187718.15	214507.63
5	0.1376	217429.81	15263.66	189756.24
6	0.1333	204793.69	124976.63	180525.31
7	0.1991	214458.41	168470.47	190017.58
8	0.0352	205437.61	160077.19	152409.12
9	0.0225	244590.33	171494.88	175243.56

10	0.0321	198963.94	102799.68	214635.18

Case 1:

In this case, the scheduling of the hybrid system without the thermodynamic characteristics and recovery cycle of the CAES facility is studied. According to Figure 2, thermal units, wind, and PV farms can participate in energy and reserve markets independently. In some hours, when the system's operator identifies that he will obtain more profit in future hours (based on price curves), he will store a part of the generated power by thermal, wind/ PV farms in the CAES facility. Furthermore, at some hours, the operator may purchase the electricity from the market for triggering the compressor. This will happen when the cost of purchasing is lower than the marginal cost of thermal units. This is explored in simulation results.

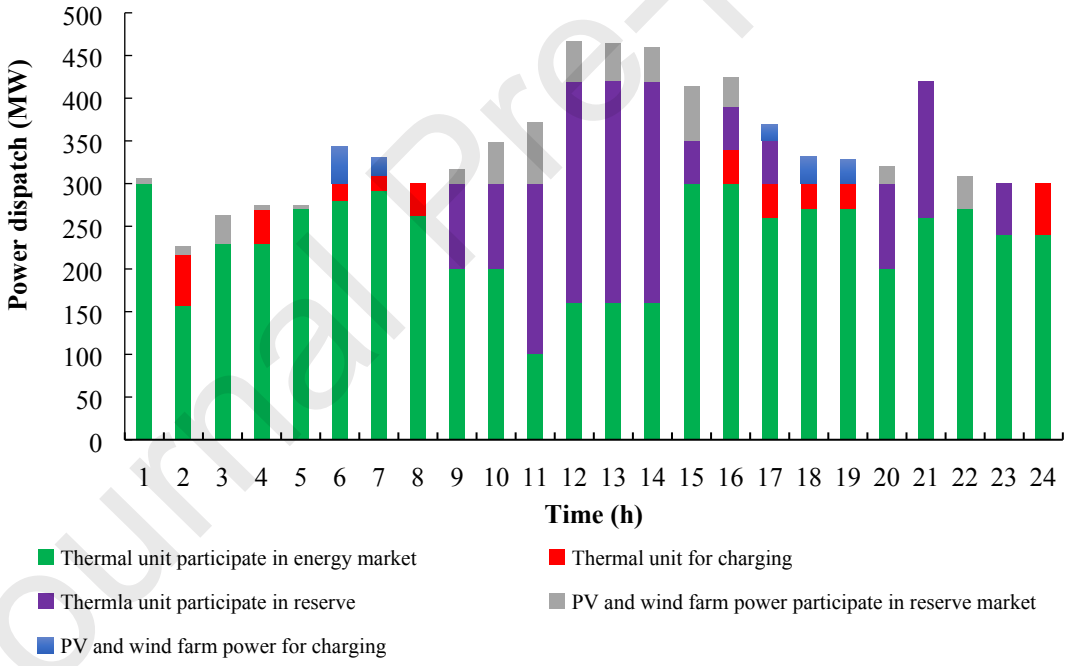

Figure. 10. The participation of thermal units, PV, and wind farms in energy and reserve markets for scenario number 7 in case 1

Figure 12 reveals the value of the participation of thermal units, wind, and PV farms in energy and reserve markets for scenario number 7. To report the generation capacity, Table V presents the power dispatch of each thermal unit for 24-hours for scenario number 7. As can be seen, units 3 and 5 are

removed from the dispatch schedule due to their high-cost coefficients. Units 1 and 2 are committed for 24-hour while units 4 and 6 are only committed for some hours.

Table IV. Thermal unit power dispatch in scenario number 7 case 1

Time	Power (MW)					
	U1	U2	U3	U4	U5	U6
1	150	150	0	0	0	0
2	150	75	0	0	0	0
3	150	75	0	0	0	0
4	150	75	0	0	0	0
5	150	150	0	0	0	0
6	150	150	0	0	0	0
7	150	150	0	0	0	0
8	150	150	0	0	0	0
9	150	150	0	0	0	0
10	150	150	0	0	0	0
11	150	150	0	0	0	0
12	150	150	0	60	0	60
13	150	150	0	60	0	60
14	150	150	0	60	0	60
15	150	150	0	0	0	0
16	150	150	0	0	0	0
17	150	150	0	0	0	0
18	150	150	0	0	0	0
19	150	150	0	0	0	0
20	150	150	0	0	0	0
21	150	150	0	60	0	60
22	150	150	0	0	0	0
23	150	150	0	0	0	0
24	150	150	0	0	0	0

Figure 13 shows the charge and discharge schemes of the CAES facility to participate in energy and reserve markets for scenario number 7. Given that the thermodynamic characteristics are neglected in this case, more flexibility in the CAES facility is observed. Consequently, it has significant participation in both markets. Except for hours 7 and 8, the CAES facility does not use the purchasing power from the market. The amount of natural gas burned in the discharging process in case 1 is 78.21 GJ. The value of profit for scenario number 7 in case 1 is $ 214458.41.

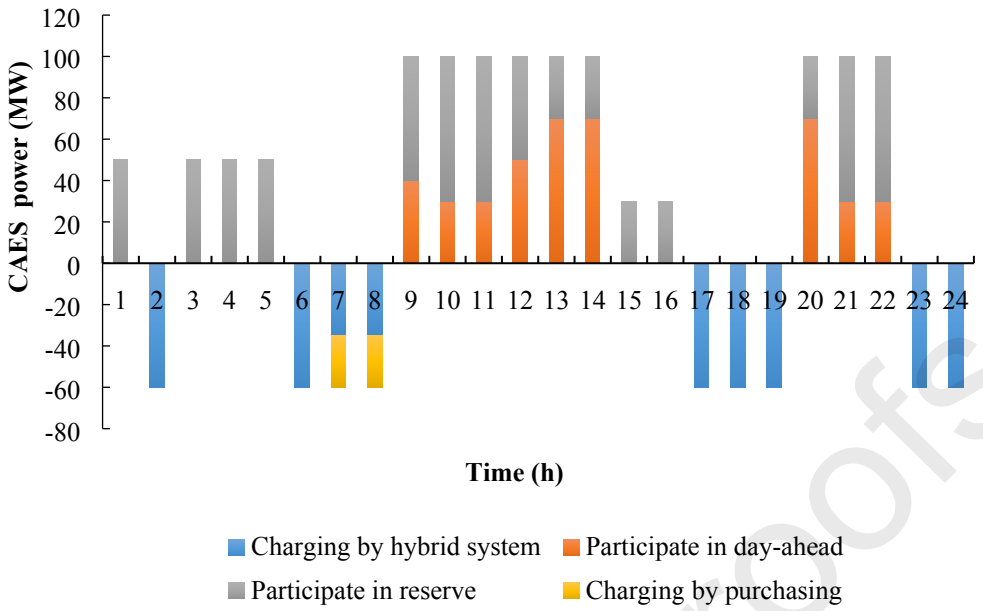

Figure. 11. CAES facility scheduling for scenario number 7 in case 1

Case 2:

The scheduling of the proposed hybrid system considering thermodynamic characteristics is studied in this case. Unlike case 1, the CAES facility scheme is affected by SoC as discussed. The operation of the system will be more realistic in this case. Figure 14 shows the CAES facility scheduling for case 2. In comparison with case 1, the facility charges more hours. Figure 14 reveals that CAES charges with 40 MW at hours 4 and 16. The main reasons for this difference from the previous case can be found in two factors. The first reason is related to partial discharging at some discharging periods. According to Figure 6, in the low level of generation, the value of the airflow rate during the discharging process is much higher due to turbine efficiency. Therefore, in the lower-level discharging, more airflow rate should be released from the cavern. So, to compensate for this gap, air should be compressed at more hours. Secondly, the effect of SoC on the compression air into the cavern, which was not considered in case 1, causes compressed air in the cavern to increase. As shown in Figure 14, the CAES facility is idle at hours 15 and 23. The reason for this is the unexpected evacuation of the cavern (when the CAES facility is discharged for consecutive hours, considering that thermodynamic characteristics lead to fast evacuation and there is no further charging and discharging possible).

Furthermore, according to Figure 7, partial discharging at discharge periods cause HR to increase. Consequently, the required fuel is higher than in case 1. Figure 15 shows the participation of wind/PV farms and thermal units in energy and reserve markets for case 2.

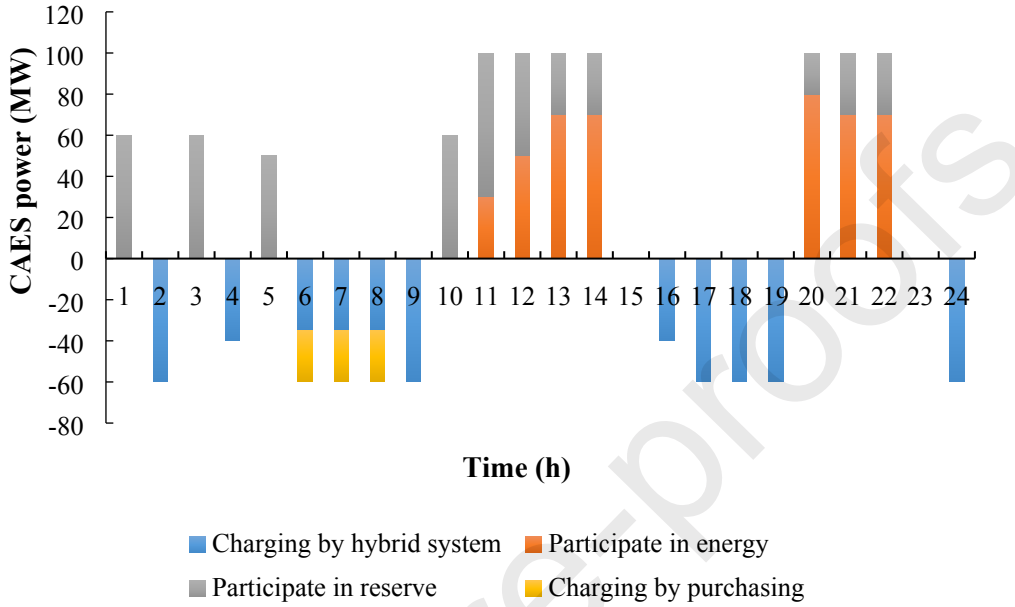

Figure. 12. CAES facility scheduling for scenario number 7 in case 2.

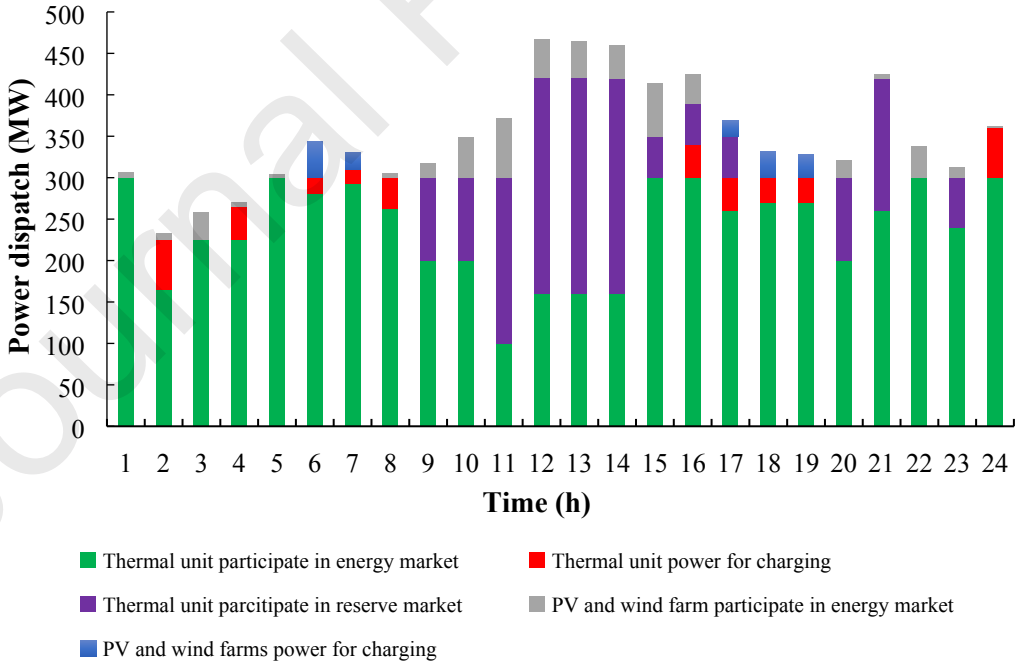

Figure. 13. The participation of thermal units, PV, and wind farms in energy and reserve markets for scenario number 7 in case 2

Table VI reports the power dispatch of thermal units for scenario number 7 in case2. In comparison with case 1, units 4 and 6 are committed more hours. Also, to provide power for the compressor, unit 3 is committed for three hours. The required natural gas and profit for scenario number 7 in case 2 are 91.41 *GJ* and $ 168470.47, respectively.

Table V. Thermal unit power dispatch for scenario number 7 in case 2

Time	Power (MW)					
	U1	U2	U3	U4	U5	U6
1	150	150	0	0	0	0
2	150	75	0	0	0	0
3	150	75	0	0	0	0
4	150	75	0	0	0	0
5	150	150	0	0	0	0
6	150	150	0	0	0	0
7	150	150	0	0	0	0
8	150	150	0	0	0	0
9	150	150	0	0	0	0
10	150	150	0	0	0	0
11	150	150	0	0	0	0
12	150	150	0	60	0	60
13	150	150	0	60	0	60
14	150	150	0	60	0	60
15	150	150	50	0	0	0
16	150	150	50	0	0	0
17	150	150	50	0	0	0
18	150	150	50	0	0	0
19	150	150	0	0	0	0
20	150	150	0	0	0	0
21	150	150	0	60	0	60
22	150	150	0	0	0	0
23	150	150	0	30	0	30
24	150	150	0	30	0	30

Case 3:

In this case, the CAES facility performance with simultaneously considering thermodynamic characteristics and recovery cycle capability is studied. The charge/discharge scheme of CAES and power dispatch of thermal units as well as the participation of the hybrid system in energy and reserve markets, are the same as case 2. However, recovery capability only affects the amount of required fuel for the combustion process. Therefore, the amount of burned fuel will change.

Figure 16 shows the variation of T_s and T_d during discharging periods while the recovery cycle is neglected (case 2). As Figure 16 shows, the operation temperature of the expander for normal

performance is about $800 \pm 50K$ while the temperature of released air from the cavern is far lower. Reach T_s to the desired temperature is carried out in the combustion chamber by adding the fuel. This process involves a major share of the system cost that comes from the purchasing of natural gas.

As previously mentioned, the turbine's exhaust gas usually at a temperature above 400-500K can be used as an energy source. As the released air from the cavern at temperature T_s passes through the recuperator, it is heated by the hot side that is fed by the exhaust gas turbine. As a result of this interaction, the outlet air of the recuperator at temperature T_b enters the burner. Figure 17 shows the variation of T_b and T_d during discharging periods considering the recovery cycle. In comparison with Figure 16, T_b is closer to the desired temperature. In other words, the required fuel to heat the released air from the cavern is less than the previous case. Based on equation (32), knowing the value of power generation at discharging periods, T_b and T_d for each discharging hour, the required fuel will be calculated.

The value of T_d is the same for Figures 16 and 17. The comparison of these figures aims to reveal the effects of the recovery cycle in the gas consumed for power generation during discharge hours. According to these figures, T_b (temperature in the presence of the recovery cycle) is much higher than T_s during discharging times. According to Figure. 16, there is almost a 200K deviation between T_b and T_s at each hour. This deviation demonstrates the effectiveness of the recovery cycle as a suitable and cost-effective resource, which results in the reduction of the gas consumed for the power generation in the expander. Consequently, the operation cost of CAES is reduced in Case 3, compared with Case 2.

The amount of required natural gas, in this case, is 81.02 GJ, which is 12% lower than case 2. The value of profit for scenario number 7 in case 3 is \$190017.58, which is 11.33% higher than case 2.

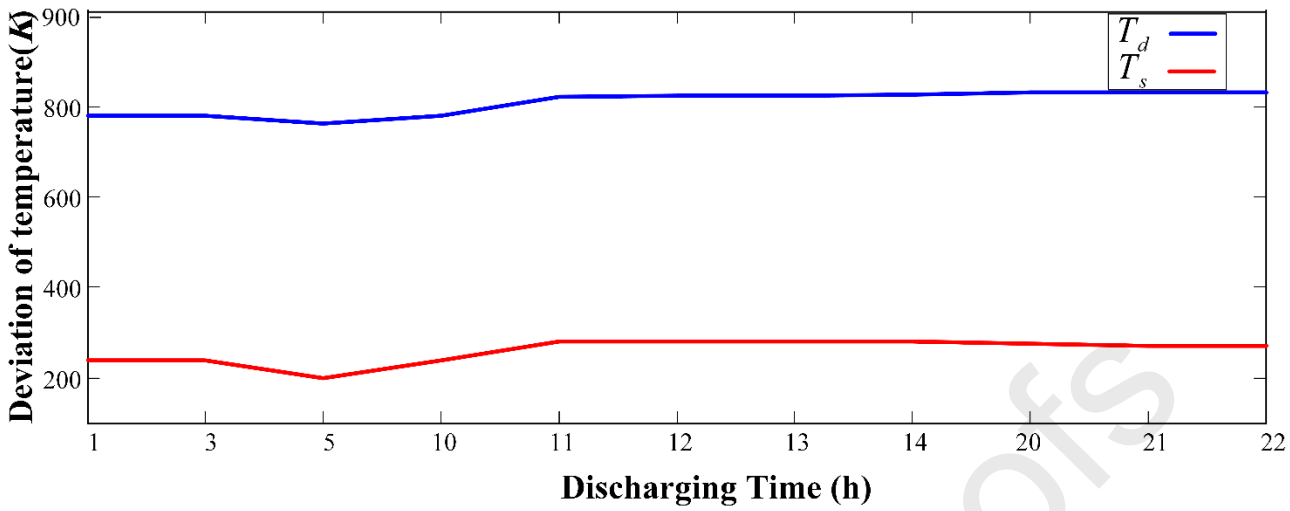

Figure. 14. The variation of T_d and T_s during discharging hour for scenario number 7

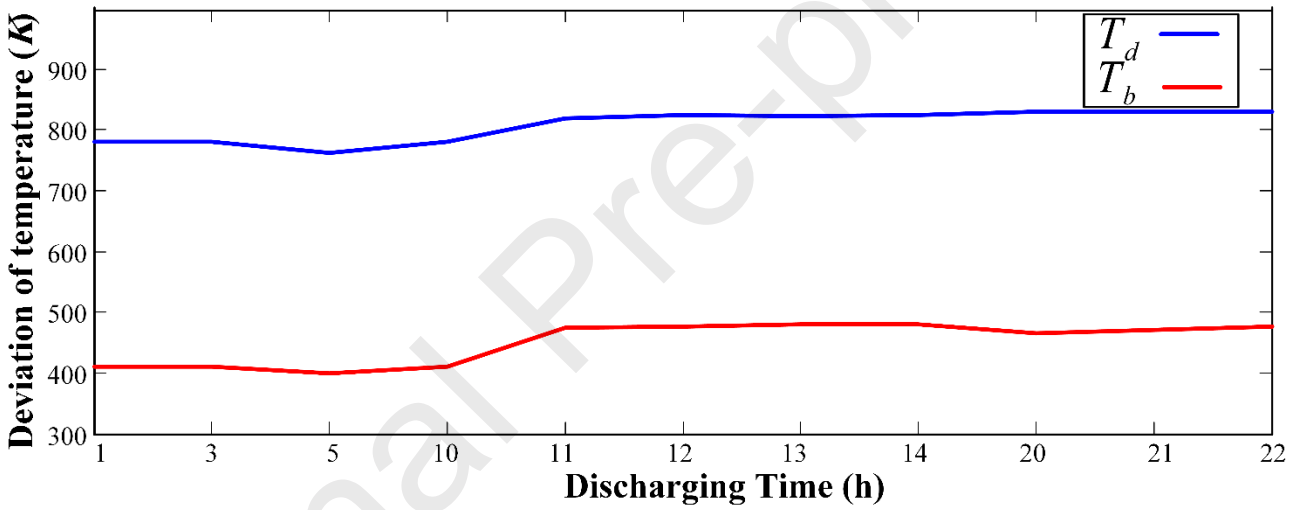

Figure. 15. The variation of T_d and T_b during discharging hour when considering the recovery cycle for scenario number 7

Briefly, we analyzed the optimal performance of the hybrid renewable-based energy system that participates in the energy and reserve markets. In case 1, the optimal operation was examined without considering the thermodynamic conditions on the CAES performance. It is obvious that in such a situation, neglecting the limitations caused by the thermodynamic assessment makes a non-realistic model, and consequently, CAES can charge/discharge with a more level of freedom. When the thermodynamic condition is considered in the model (case 2, CAES operates more realistic and in addition to the previous limits, thermodynamical constraints should be established, too. Hence, optimal

charging/ discharging values changes. Finally, considering the recovery cycle in the CAES operation in case 3 reveals the effectiveness of this capability from the burned natural gas point of view. In other words, the optimal scheme of the CAES does not change in comparison with case 2. However, the required natural gas for the combustion is significantly reduced due to the higher inlet air temperature to the burner. Table VII compares the major results of three cases. According to Table VII, considering the thermodynamic condition in the model reduces the daily profit up to 21.4% while provides a more realistic model compared with case 1. Also, considering the recovery cycle and thermodynamic condition for the CAES coupled with renewable energy in the hybrid system reduces the required natural gas for the combustion up to 11.33%, and improves the profit up to 11.36%.

Table VII. Comparison of major results in studied cases

	Profit ($)	Changes (%)	Consumed natural gas (GJ)	Changes (%)
Case 1	214458.41	———	78.21	———
Case 2	168470.47	-21.4%*	91.41	-14.4%*
Case 3	190017.58	11.36%*	81.02	11.33%*

* compared with the previous case

Validation of results

For validating the simulation results in case studies, several experiments with different input data, such as expander and turbine outlet temperature, cavern capacity, and price data, have been done.

Table VIII shows the optimal daily profit of the proposed hybrid system for different expander temperature. As discussed, the recovery cycle can be considered as the main heat resource. In case 3, we supposed that the outlet temperature of the expander is about 800 *k*. however, this value can affect the T_b, results in consumed natural gas, consequently profit. According to Table VIII, as the expander temperature increases, T_b increase, consequently, the profit has risen. For example, for $T_d = 1000k$, the T_b equals 590, and profit increases to $ 237701.86 (25% higher compared with case 3).

The optimal scheduling of the hybrid system is analyzed for different price curves based on the valid power markets. As discussed, the optimal charge/discharge and power exchanging in studied cases are obtained according to Figure 10. However, using price data given by universal power markets valid the simulation results. To this end, the numerical results of case number 3 are repeated for PJM, ERCOT, and NYISO day-ahead markets [46] which are provided in Table IX. According to this table, the proposed bidding strategy of the hybrid energy system considering the thermodynamic condition is compatible with different energy markets.

Finally, for validating the simulation results, several cavern capacity per mass of the air is captured. Table X indicates the effects of the cavern capacity on the minimum SoC and profit. Numerical results in three case studies are presented for minimum SoC 31%, and $AM^{\max}$ 9.8 million kg. However, these values affect the inlet and outlet air flow rate, cavern SoC, turbine efficiency, as well as total profit. According to Table X, as the cavern capacity decreases, the minimum SoC increase. This means that lower air can be stored in the cavern. Also, for $AM^{\max}=10$ million kg, the minimum SoC equals 27%, and the maximum profit can be achieved. It should be noted that the more increasing of the cavern capacity due to the thermodynamic condition during the charging and discharging modes, as well as cavern pressure, has an inverse effect on the profit as can be seen from Table X.

The presented comparison in Tables VII, IX, and X validate the numerical simulation results based on the different input data.

Table VIII. Analyzing the effects of the recovery cycle on the profit for different value of T_d

Expander temperature (K)	T_b	Profit ($)
750	382	175319.51
850	471	208537.43
900	535	219340.06
1000	593	237701.8

Table IX. Validation of obtained profit for different power market

Markets	Day-ahead PJM	Day-ahead ERCOT	Day-ahead NYISO
Profit ($)	192431.82	189537.54	195442.5

Table X. Analyzing the effects of cavern capacity on the minimum SoC and total profit

The maximum mass of air in a cavern (million kg)	Minimum SoC (%)	Profit ($)
9	38	185351.71
10	27	214391.82
11	24	197304.77

V. Conclusion

This paper developed the thermodynamic modeling of compressed air energy storage incorporated with wind and photovoltaic farms, as well as thermal units in the novel hybrid system. Considering thermodynamic characteristics of CAES for both charging and discharging mode, resulting in an hourly cavern state of charge, which was a function of the inlet/ outlet airflow rate, cavern pressure, and efficiency of compressor and turbines. Also, the recovery cycle capability was embedded for CAES to enable the utilization of exhaust wasted air as a heat resource based on the comprehensive mathematical formulation. The proposed hybrid system has participated in both energy and reserve markets with the aim of profit maximization. To capture high-level existing uncertainty, including energy and reserve market prices, as well as wind and PV power output, a scenario-based stochastic approach based on real historical data of KHAF station in IRAN was implemented. The major conclusions from numerical results can be outlined as follows:

- Applying the thermodynamic characteristics for CAES operation makes the proposed scheduling more realistic.
- Considering thermodynamic characteristics makes significant changes in hourly charging/ discharging schemes, which result in less profit comparison up to 21.4%.
- Incorporating the recovery cycle capability in the CAES performance results in a significant reduction in burned natural gas up to 11.33%, and improve the system profit by up to 12 %.

However, the development of the proposed hybrid system with other uncertainty modeling frameworks such as information gas decision theory and robust optimization approach, as well as providing the participation in the natural gas market beside electricity markets, have remained for future works.

VI. Acknowledgment

The authors acknowledge the support of the "Optimal Operation of Natural Gas and Reconfigurable Electricity Networks in the presence of Connected Energy Hub to Network" project funded by the Iran National Science Foundation (INSF) under Grant No. 99012662.

References

[1] "EPRI's Energy Storage Roadmap, Vision for 2025," 2020.

[2] V. Dreißigacker and S. Belik, "High temperature solid media thermal energy storage system with high effective storage densities for flexible heat supply in electric vehicles," *Applied Thermal Engineering,* vol. 149, pp. 173-179, 2019.

[3] M. A. Mirzaei, M. Hemmati, K. Zare, B. Mohammadi-Ivatloo, M. Abapour, M. Marzband*, et al.*, "Two-stage robust-stochastic electricity market clearing considering mobile energy storage in rail transportation," *IEEE Access,* vol. 8, pp. 121780-121794, 2020.

[4] C. Sundarabalan, N. Tejasree, R. V. Shankar, Y. Puttagunta, and V. Vignesh, "Compressed air energy storage powered dynamic voltage restorer for voltage compensation in three-phase distribution system," *Sustainable Cities and Society,* vol. 46, p. 101420, 2019.

[5] M. Abbaspour, M. Satkin, B. Mohammadi-Ivatloo, F. H. Lotfi, and Y. Noorollahi, "Optimal operation scheduling of wind power integrated with compressed air energy storage (CAES)," *Renewable Energy,* vol. 51, pp. 53-59, 2013.

[6] A. S. Alsagri, A. Arabkoohsar, H. R. Rahbari, and A. A. Alrobaian, "Partial load operation analysis of trigeneration subcooled compressed air energy storage system," *Journal of Cleaner Production,* vol. 238, p. 117948, 2019.

[7] J. Chen, W. Liu, D. Jiang, J. Zhang, S. Ren, L. Li*, et al.*, "Preliminary investigation on the feasibility of a clean CAES system coupled with wind and solar energy in China," *Energy,* vol. 127, pp. 462-478, 2017.

[8] S. Shafiee, H. Zareipour, A. M. Knight, N. Amjady, and B. Mohammadi-Ivatloo, "Risk-constrained bidding and offering strategy for a merchant compressed air energy storage plant," *IEEE Transactions on Power Systems,* vol. 32, pp. 946-957, 2017.

[9] A. Attarha, N. Amjady, S. Dehghan, and B. Vatani, "Adaptive Robust Self-scheduling for a Wind Producer with Compressed Air Energy Storage," *IEEE Transactions on Sustainable Energy,* 2018.

[10] P. Aliasghari, M. Zamani-Gargari, and B. Mohammadi-Ivatloo, "Look-ahead risk-constrained scheduling of wind power integrated system with compressed air energy storage (CAES) plant," *Energy,* vol. 160, pp. 668-677, 2018.

[11] A. Mohammadi and M. Mehrpooya, "Exergy analysis and optimization of an integrated micro gas turbine, compressed air energy storage and solar dish collector process," *Journal of Cleaner Production,* vol. 139, pp. 372-383, 2016.

[12] A. Razmi, M. Soltani, C. Aghanajafi, and M. Torabi, "Thermodynamic and economic investigation of a novel integration of the absorption-recompression refrigeration system with compressed air energy storage (CAES)," *Energy Conversion and Management,* vol. 187, pp. 262-273, 2019.

[13] H. Meng, M. Wang, O. Olumayegun, X. Luo, and X. Liu, "Process design, operation and economic evaluation of compressed air energy storage (CAES) for wind power through modelling and simulation," *Renewable energy,* vol. 136, pp. 923-936, 2019.

[14] A. N. Ghalelou, A. P. Fakhri, S. Nojavan, M. Majidi, and H. Hatami, "A stochastic self-scheduling program for compressed air energy storage (CAES) of renewable energy sources (RESs) based on a demand response mechanism," *Energy conversion and management,* vol. 120, pp. 388-396, 2016.

[15] S. Shafiee, H. Zareipour, and A. Knight, "Considering thermodynamic characteristics of a CAES facility in self-scheduling in energy and reserve markets," *IEEE Transactions on Smart Grid,* 2016.

[16] P. Zhao, L. Gao, J. Wang, and Y. Dai, "Energy efficiency analysis and off-design analysis of two different discharge modes for compressed air energy storage system using axial turbines," *Renewable Energy,* vol. 85, pp. 1164-1177, 2016.

[17] M. Zeynalian, A. H. Hajialirezaei, A. R. Razmi, and M. Torabi, "Carbon dioxide capture from compressed air energy storage system," *Applied Thermal Engineering,* vol. 178, p. 115593, 2020.

[18] P. Wang, P. Zhao, W. Xu, J. Wang, and Y. Dai, "Performance analysis of a combined heat and compressed air energy storage system with packed bed unit and electrical heater," *Applied Thermal Engineering,* vol. 162, p. 114321, 2019.

[19] J. Fan, H. Xie, J. Chen, D. Jiang, C. Li, W. N. Tiedeu*, et al.*, "Preliminary feasibility analysis of a hybrid pumped-hydro energy storage system using abandoned coal mine goafs," *Applied Energy,* vol. 258, p. 114007, 2020.

[20] S. Houssainy, M. Janbozorgi, P. Ip, and P. Kavehpour, "Thermodynamic analysis of a high temperature hybrid compressed air energy storage (HTH-CAES) system," *Renewable energy,* vol. 115, pp. 1043-1054, 2018.

[21] B. Llamas, C. Laín, M. C. Castañeda, and J. Pous, "Mini-CAES as a reliable and novel approach to storing renewable energy in salt domes," *Energy,* vol. 144, pp. 482-489, 2018.

[22] H. Guo, Y. Xu, Y. Zhang, Q. Liang, H. Tang, X. Zhang*, et al.*, "Off-design performance and an optimal operation strategy for the multistage compression process in adiabatic compressed air energy storage systems," *Applied Thermal Engineering,* vol. 149, pp. 262-274, 2019.

[23] Y. Li, S. Miao, S. Zhang, B. Yin, X. Luo, M. Dooner*, et al.*, "A reserve capacity model of AA-CAES for power system optimal joint energy and reserve scheduling," *International Journal of Electrical Power & Energy Systems,* vol. 104, pp. 279-290, 2019.

[24] F. de Bosio and V. Verda, "Thermoeconomic analysis of a Compressed Air Energy Storage (CAES) system integrated with a wind power plant in the framework of the IPEX Market," *Applied Energy,* vol. 152, pp. 173-182, 2015.

[25] I. Calero, C. A. Canizares, and K. Bhattacharya, "Compressed Air Energy Storage System Modeling for Power System Studies," *IEEE Transactions on Power Systems,* 2019.

[26] S. Wu, C. Zhou, E. Doroodchi, and B. Moghtaderi, "Thermodynamic analysis of a novel hybrid thermochemical-compressed air energy storage system powered by wind, solar and/or off-peak electricity," *Energy conversion and management,* vol. 180, pp. 1268-1280, 2019.

[27] M. J. Ghadi, A. Azizivahed, A. Rajabi, S. Ghavidel, L. Li, J. Zhang*, et al.*, "Day-Ahead Market Participation of an Active Distribution Network Equipped with Small-Scale Compressed Air Energy Storage Systems," *IEEE Transactions on Smart Grid,* 2020.

[28] J. Moradi, H. Shahinzadeh, A. Khandan, and M. Moazzami, "A profitability investigation into the collaborative operation of wind and underwater compressed air energy storage units in the spot market," *Energy,* vol. 141, pp. 1779-1794, 2017.

[29] Z. Liu, Z. Liu, X. Xin, and X. Yang, "Proposal and assessment of a novel carbon dioxide energy storage system with electrical thermal storage and ejector condensing cycle: Energy and exergy analysis," *Applied Energy,* vol. 269, p. 115067, 2020.

[30] Z. Liu, Z. Liu, X. Cao, T. Luo, and X. Yang, "Advanced exergoeconomic evaluation on supercritical carbon dioxide recompression Brayton cycle," *Journal of Cleaner Production,* vol. 256, p. 120537, 2020.

[31] Z. Liu, B. Liu, J. Guo, X. Xin, and X. Yang, "Conventional and advanced exergy analysis of a novel transcritical compressed carbon dioxide energy storage system," *Energy Conversion and Management,* vol. 198, p. 111807, 2019.

[32] M. Marchionni, G. Bianchi, and S. A. Tassou, "Review of supercritical carbon dioxide (sCO 2) technologies for high-grade waste heat to power conversion," *SN Applied Sciences,* vol. 2, pp. 1-13, 2020.

[33] M. Marchionni, G. Bianchi, K. M. Tsamos, and S. A. Tassou, "Techno-economic comparison of different cycle architectures for high temperature waste heat to power conversion systems using CO2 in supercritical phase," *Energy Procedia,* vol. 123, pp. 305-312, 2017.

[34] A. Sciacovelli, D. Smith, M. Navarro, A. Vecchi, X. Peng, Y. Li*, et al.*, "Performance analysis and detailed experimental results of the first liquid air energy storage plant in the world," *Journal of Energy Resources Technology,* vol. 140, 2018.

[35] A. Sciacovelli, A. Vecchi, and Y. Ding, "Liquid air energy storage (LAES) with packed bed cold thermal storage–From component to system level performance through dynamic modelling," *Applied Energy,* vol. 190, pp. 84-98, 2017.

[36] M. Hemmati, M. Abapour, B. Mohammadi-Ivatloo, and A. Anvari-Moghaddam, "Optimal Operation of Integrated Electrical and Natural Gas Networks with a Focus on Distributed Energy Hub Systems," *Sustainability,* vol. 12, p. 8320, 2020.

[37] R. Kaviani, M. Rashidinejad, and A. Abdollahi, "A milp igdt-based self-scheduling model for participating in electricity markets," in *2016 24th Iranian Conference on Electrical Engineering (ICEE)*, 2016, pp. 152-157.

[38] M. A. Mirzaei, M. Hemmati, K. Zare, M. Abapour, B. Mohammadi-Ivatloo, M. Marzband*, et al.*, "A novel hybrid two-stage framework for flexible bidding strategy of reconfigurable micro-grid in day-ahead and real-time markets," *International Journal of Electrical Power & Energy Systems,* vol. 123, p. 106293, 2020.

[39] E. A. Saputro and M. M. Farid, "A novel approach of heat recovery system in compressed air energy storage (CAES)," *Energy conversion and management,* vol. 178, pp. 217-225, 2018.

[40] Z.-S. Zhang, Y.-Z. Sun, J. Lin, L. Cheng, and G.-J. Li, "Versatile distribution of wind power output for a given forecast value," in *Power and Energy Society General Meeting, 2012 IEEE*, 2012, pp. 1-7.

[41] http://suna.org.ir/ationoffice-windenergyoffice-windamar-fa.html.

[42] X. Dui, G. Zhu, and L. Yao, "Two-stage optimization of battery energy storage capacity to decrease wind power curtailment in grid-connected wind farms," *IEEE Transactions on Power Systems,* vol. 33, pp. 3296-3305, 2018.

[43] M. Hemmati, B. Mohammadi-Ivatloo, M. Abapour, and A. Anvari-Moghaddam, "Day-ahead profit-based reconfigurable microgrid scheduling considering uncertain renewable generation

and load demand in the presence of energy storage," *Journal of Energy Storage,* vol. 28, p. 101161, 2020.

[44] M. Hemmati, B. Mohammadi-Ivatloo, M. Abapour, and A. Anvari-Moghaddam, "Optimal Chance-Constrained Scheduling of Reconfigurable Microgrids Considering Islanding Operation Constraints," *IEEE Systems Journal,* 2020.

[45] https://www.energymarketprice.com.

[46] www.energyonline.com.

Declaration of interests

☒ The authors declare that they have no known competing financial interests or personal relationships that could have appeared to influence the work reported in this paper.

☐The authors declare the following financial interests/personal relationships which may be considered as potential competing interests:

- Thermodynamically modeling of CAES integrated with wind, PV, and thermal units
- Participate in multi energy markets considering thermodynamically of CAES
- Proposing a heat recovery cycle to increase the efficiency of the CAES systems
- Using a stochastic method to model renewable power, energy and reserve prices